Letter of Intent

FLARE

Fermilab Liquid ARgon Experiments

Version 1.0

August 25, 2004

Bartoszek Eng. - Duke - Indiana - Fermilab - LSU - MSU -
Osaka - Pisa - Pittsburgh - Princeton - Silesia   South Carolina - Texas A&M -
Tufts - UCLA - Warsaw University -
INS Warsaw - Washington - York-Toronto

L. Bartoszek
Bartoszek Engineering

K. Scholberg
Duke University, Durham, NC

R. Tayloe, G. Visser
Indiana University, Bloomington, IN

B.T. Fleming, G.F. Foster,R. Hatcher, W. Jaskierny,
H. Jostlein, C. Kendziora, J. Kilmer, K. Krempetz,
V. Makeev, A. Marchionni, A. Para[†], S. Pordes, P. Rapidis,
R. Schmitt, Z. Tang, B. Wands
Fermilab, Batavia, IL

W. Metcalf, M.0. Wascko
Louisiana State University, Baton Rouge, LA

C. Bromberg, R. Richards
Michigan State University, East Lansing, MI

H. Ejiri, M. Nomachi, R. Hazama
Osaka University, Osaka, Japan

F. Sergiampietri[1]
INFN,Pisa, Italy

D. Naples
University of Pittsburgh, Pittsburgh, PA

K. T. McDonald
Princeton University, Princeton, NJ

J. Czakanski
University of Silesia, Katowice, Poland

A. Godley, S.R. Mishra, C. Rosenfeld, K. Wu
University of South Carolina, Columbia, SC

J.T. White
Texas A&M University, College Station, TX

A. Mann, W.P. Oliver, J. Schneps

Tufts University, Boston, MA

D. Cline, S. Otwinowski, Y. Seo, H. Wang
UCLA, Los Angeles, CA

J. Stepaniak
Institute for Nuclear Studies, Warsaw, Poland

W. Dominik
Warsaw University, Warsaw, Poland

P.J. Doe, J. Formaggio, R.G.H. Robertson, J.F. Wilkerson
University of Washington, Seattle

S. Menary
York University, Toronto, Canada

[†] **Contact person**
[1] Also UCLA, Los Angeles, CA

Contents

Executive summary

Neutrinos have been a source of excitement lately. While the neutrino mixing has been expected, its pattern has taken us by surprise. The first evidence of physics beyond the standard model is here and more excitement is likely on the way..

Fermilab has a unique opportunity to take a lead in the neutrino physics in the next decade or so. Our recent major investments put us in an enviable position of having two intense neutrino beams with energies spanning the range from 0.5 GeV to 20 GeV. To exploit fully our investment we need new experiment(s) matching the physics potential of our neutrino beams.

Some of the most compelling questions can be addressed with a Fermilab, long baseline, off-axis experiment. A fortunate combination of the NuMI off-axis beam spectrum and the emerging value of Δm_{32}^2 makes the distances offered by the NuMI beam nearly optimal for the ν_e appearance experiment, which is the key to the most interesting questions:

- what is the pattern of neutrino masses? "normal" or "inverted" hierarchy?

- what is the value of the mixing angle $\sin^2 2\theta_{13}$?

- is CP violated in the neutrino sector?

We are very fortunate that a new powerful detector technology has been developed recently. This technology, the Liquid Argon Time Projection Chamber, is just waiting to be exploited. The Liquid Argon Time Projection Chamber is a relatively inexpensive detector ideally matched to the need of neutrino experiments. It provides a bubble-chamber like view of interactions thus enabling very efficient detection and classification of neutrino interactions. The long R&D effort of the ICARUS collaboration culminated in the successful operation of a 300 ton detector. Using the technology demonstrated by the ICARUS group one can construct a wide variety of neutrino experiments.

The physics potential of neutrino beams is limited by the statistics of the available event sample which is proportional to a product of the beam intensity, the detector mass and the detection efficiency. While it is important to maximize the beam intensity it is equally important to take full advantage of the available beam by maximizing the detector mass and the detection efficiency. The high detection efficiency of a liquid argon detector makes its physics potential equivalent to that of a conventional detector with the beam power upgraded by the proton driver.

New, intense neutrino beams and advanced detection techniques have rekindled interest in conventional neutrino scattering physics. This physics is interesting in its own right, but improved knowledge in this area will also be necessary for precise measurements of the neutrino oscillation parameters.

A very large, 50 kton class, surface detector at the far location in the NuMI beam will enable sensitive measurements of the neutrino oscillation parameters. Its superb spatial granularity may make it possible to detect supernovae and determine the resulting neutrino spectrum. It may even detect protons decaying into kaons, should any of these events occur during the lifetime of the experiment.

Small, 40 ton class, liquid argon detectors exposed to the MiniBOONE and NuMI beams at the close locations will provide a wealth of physics results, thus filling a hole in our knowledge of neutrino physics at low energies.

Is the neutrino a Dirac or a Majorana particle? This fundamental question awaits an experimental answer and neutrino-less double beta decay experiments are the way to provide it. These experiments require very high background rejection and excellent energy resolution to fight the background of a normal double beta decay. The Liquid Argon TPC provides both, thus making it a very attractive candidate for the technology of the next generation of experiments.

The Liquid Argon TPC appears to be a very versatile and very powerful technology applicable to a wide range of physics experiments. The fundamentals of the experimental techniques have been established and, in principle, one can design small or large detectors as physics demands. We feel, however, that more practical experience is necessary to make such experimental proposals credible.

In the case of small detectors, the necessary R&D is limited to technology transfer and gaining some practical experience. Credible proposals for a very large detector require engineering studies of the application of the fundamental technology on a very large scale. This is especially important to confirm the credibility of cost estimates for such a detector. A double beta decay version of a liquid argon detector also requires further studies of energy resolution at the very low energy end.

Liquid Argon TPC detectors can greatly enhance the physics reach of the neutrino program at Fermilab. They can also be of significant importance for neutrino programs in future underground laboratories. Therefore we consider it necessary to embark on a vigorous program of detector studies to establish credible designs of physics experiments. Fermilab, with its mix of technical resources and a long tradition of liquid argon detectors, is a natural place for such studies.

The physics motivation and technical aspects of a Liquid Argon R&D program are laid out in the following chapters:

- Chapter 1 describes the potential of a 50 kton off-axis detector for studies of neutrino oscillations

- Chapter 2 discusses the potential of a large surface detector to detect supernova neutrinos and proton decay

- Chapter 3 describes the physics potential of 40 ton detectors in the NuMI and MiniBOONE beams

- Chapter 4 describes the fundamentals of the Liquid Argon TPC and the demonstration of its practical implementation by the ICARUS collaboration

- Chapter 5 describes a 50 kton off-axis detector and discusses technical aspects and cost estimates

- Chapter 6 describes a design of a 40 ton detector, suitable for the near location at NuMI or MiniBOONE beams

- Chapter 7 describes a possible application of liquid argon technology for a neutrino-less double beta decay experiment

- Chapter 8 outlines a possible program of technology transfer, engineering studies and possible improvements of the detector technology

Chapter 1

Neutrino Oscillations Studies with the Off-axis Liquid Argon Detector

1.1 Studies of Neutrino Oscillations: The Physics Case

Neutrinos have mass and oscillate. There are two oscillation frequencies driven by the two mass differences of neutrino mass eigenstates: Δm_{12}^2 and Δm_{32}^2. Interference of these two processes is expected to produce measurable CP violating effects.

The oscillation at the "atmospheric" mass difference Δm_{32}^2 is a subject of studies with long baseline neutrino experiments, the maximum of oscillations occurring at $E_\nu = \frac{2.54}{\pi} L \Delta m_{32}^2$. To set the scale: taking the current estimate of $\Delta m_{32}^2 = 2.5 \times 10^{-3} \ eV^2$ and a distance $L = 850 \ km$ the oscillation maximum occurs at $E_\nu = 1.7 \ GeV$.

Recent developments in neutrino physics have established that, contrary to the expectations, at least two neutrino mixing angles, $\sin^2 2\theta_{12}$ and $\sin^2 2\theta_{23}$ are very large. The latter is consistent with being the maximal, hence raising a tantalizing possibility that some new, hereto unknown symmetry of nature may be at work here. Precise measurement of the deviation of this angle from its maximal value is, therefore, of great importance.

Neutrino oscillation experiments have established that neutrino masses exhibit a pattern of a doublet of closely spaced masses, m_1 and m_2, whereas the third mass is much further apart. A natural question arises what is the pattern of neutrino masses? Is it 'normal', with $m_1 < m_2 \ll m_3$, or 'inverted', with $m_3 \ll m_1 < m_2$ hierarchy? This question can be answered experimentally in the $\nu_\mu \to \nu_e$ appearance experiment with neutrino and antineutrino beams, as the the matter effects change the transition rates differently.

While 'solar' (including long baseline reactor experiment) and atmospheric neutrino experiments have established that the electron neutrino is predominantly composed of m_1 and m_2 mass eigenstates there might be some admixture of the ν_e in the third state m_3. The size of his admixture is known to be not very large, $\sin^2 2\theta_{13} \leq 0.12$, but its precise value is of great interest. It has a significant power to discriminate between various theoretical models of neutrino mixing but more importantly, its size determines the practical observability of the CP violating effects in the long baseline experiments.

It is quite fortunate that all of the emerging questions can be addressed by a single experiment, that of $\nu_\mu \to \nu_e$ oscillations. This is well illustrated on the 'bi-probability' plots[39] shown in Fig.1.1. The experimental results can be expressed as two numbers: P_ν and $P_{\bar\nu}$ being the probabilities of the $\nu_\mu \to \nu_e$ transitions in a given detector configuration for a neutrino and antineutrino beams respectively. A distance of the resulting data point is a measure of the mixing angle $\sin^2 2\theta_{13}$. In a CP-conserving world and a vacuum experiment the result must lie on a diagonal. Matter effects will displace the result to be below or above the diagonal for the "normal" and "inverted" hierarchy respectively. The presence of th CP violating phase will move the result to in point on the ellipse,its exact location related to the value of the phase.

At the larger values of $\sin^2 2\theta_{13}$ the ellipses associated with the two possible mass hierarchies separate in matter, whereas they are approximately degenerate in vacuum. There is also a significant sensitivity to the CP violating phase, δ. It is the sensitivity to the sign of Δm^2_{32} and the CP violating phase in these plots which allows for the determination of these parameters in a sufficiently accurate experiment. For a single experiment there can be a degeneracy in the determined parameters but this degeneracy can be broken by further experimentation.

1.2   The NuMI Opportunity

The NuMI neutrino beam was designed to address the "atmospheric neutrino anomaly". By a fortunate coincidence its off-axis components[40, 41] provide an unique opportunity to study the emerging questions in the neutrino sector. The NuMI beam allows for experiments with a baseline between 700 km and 950 km. The detector distance from the nominal beam axis determines the resulting beam energy and spectral shape.

The current values of the oscillation parameters indicate that the oscillation maximum, at the NuMI distances, occurs at the neutrino energies of the order of 2 GeV. This is very fortunate, as this energy corresponds to the decay angle of about 90° in the center-of-mass of the decaying pion frame, hence the beam intensity is relatively high. The expected events rates, in the absence of oscillations, are in the range of 100 $events/kton/year$. Narrow energy spectrum helps to reduce the backgrounds from possible neutral current interactions.

The irreducible background for the ν_e oscillation experiment is due to the ν_e component of the beam. The ν_e flux is of the order of 0.5% of the ν_μ flux[42] in the region of interest. In this region the ν_e flux is primarily produced
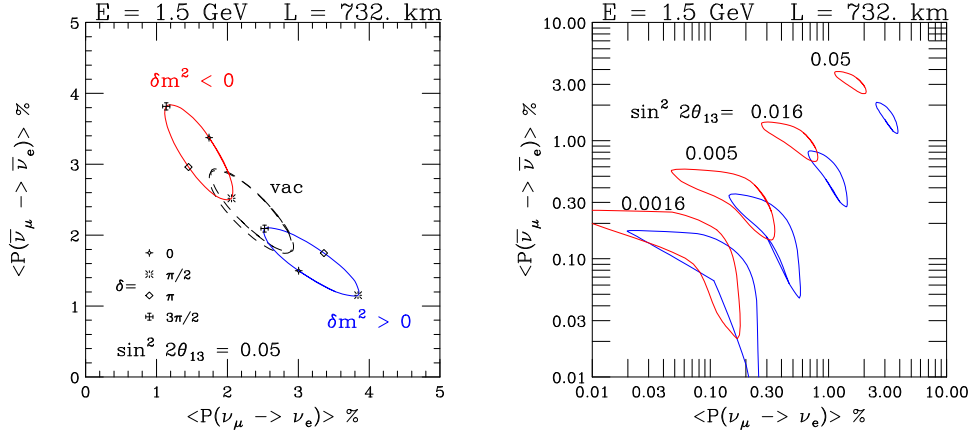
Figure 1.1: The bi-probability plots $P(\nu_\mu \to \nu_e)$ versus $P(\bar{\nu}_\mu \to \bar{\nu}_e)$ assuming a constant matter density of $\rho = 3.0 g cm^{-3}$ for an L/E of 500 km/GeV. The mixing parameters are fixed to be $|\Delta m^2_{31}| = 3 \times 10^{-3} eV^2$, $\sin^2 2\theta_{23} = 1.0$, $\Delta m^2_{21} = +5 \times 10^{-5} eV^2$, $\sin^2 2\theta_{12} = 0.8$ with the labeled values of $\sin^2 2\theta_{13}$ and δ.

by secondary muons decay, the same muons which accompany the main ν_μ component of the beam. It is expected hat the MINOS near detector, as well as possible dedicated near detectors will determine this background with an accuracy of few percent.

1.3 Experimental Aspects of the ν_e Appearance

The experimental challenge is to detect and identify charged current ν_e interactions resulting from the $\nu_\mu \to \nu_e$ oscillations. The signal events are characterized by the presence of an electrons in the final state. The total energy of the final state particles is a measure of the neutrino energy. A characteristic feature of the charged current interactions, as opposed to the neutral current ones, is the balance of the transverse momentum, up to a small contribution from the Fermi motion of target nucleons.

The irreducible background of from the ν_e component of the beam has the same characteristics and it is indistinguishable from the signal in every detector. The only factor allowing to minimize this component of the background is the total energy resolution, due to the fact the the signal events have their energy distribution peaked sharply in the region of the maximum flux of the neutrino beam whereas the background ν_e events have rather flat energy distribution.

The second contribution of the background is caused by events with no primary electron, but the produced π^0 or a photon conversion is mistakenly identified as an electron in neutral or ν_μ charged current interactions. The latter category is relatively suppressed as only the events with a muon not identified as such will be classified as potential signal candidates.

The "fake" electrons rejection is the primary experimental challenge of the experiment and it determines the physics potential of the experiment. On one hand the presence of the π^0 background increases the background level, on the other hand a requirement to keep it at tolerable levels leads to analysis cuts reducing the efficiency for the signal detection.

The physics potential of an experiment (with a given beam and at a given location) can be expressed in terms of

$$FOM = \frac{\varepsilon S}{\sqrt{\varepsilon(S + B_{beam}) + B_{\pi^0}}} \tag{1.1}$$

where S is the number of the events expected from the oscillations, B_{beam} is a number of CC ν_e interactions produced by the ν_e beam component, ε is the efficiency for the detection and identification of ν_e CC interactions and B_{π^0} is the number of non-ν_e interactions classified as signal candidates under the cuts giving the ε efficiency.

It is expected that the background levels will be determined with high accuracy and the physics reach of the experiment will be limited by the statistical fluctuations of the otherwise well known background. In such a situation $FOM \sim \sqrt{MtN_P}$ where M is the detector mass, t is the running time and N_P is the number of protons delivered onto the neutrino target.

Several independent studies have shown that in the case of high granularity sampling detectors the optimum of the physics potential is reached when the π^0 induced background is of about the same size as the intrinsic ν_e background and that such an analysis typically has efficiency,ε, of about 30%.

A major improvement can be achieved with imaging detectors, like a liquid argon TPC, which allow for nearly complete elimination of the π^0 induced background and, at the same time, high efficiency of the ν_e identification, of the order of 90%. The desired level of reduction of the π^0 induced background is set by a requirement $\varepsilon B_{beam} \gg B_{\pi^0}$. Further reduction contributes little to the FOM as the statistical fluctuations of the irreducible background dominate.

The increase of the physics potential of the imaging detector over the sampling calorimeter depends somewhat on the physics scenario. If the osculation signal is large, hence $\varepsilon S \gg \varepsilon B_{beam} + B_{\pi^0}$ than the liquid argon detector of a given mass is equivalent to three times larger conventional detector, thanks to excellent electron identification efficiency. The ultimate sensitivity of the liquid argon detector, corresponding to the case $\varepsilon S \ll \varepsilon B_{beam} + B_{\pi^0}$, is equal to that of six times bigger conventional detector, or of the conventional detector with a new proton driver-driven beam, thanks to an additional reduction of the background by a factor of two.

High detection and identification efficiency has an additional advantage of
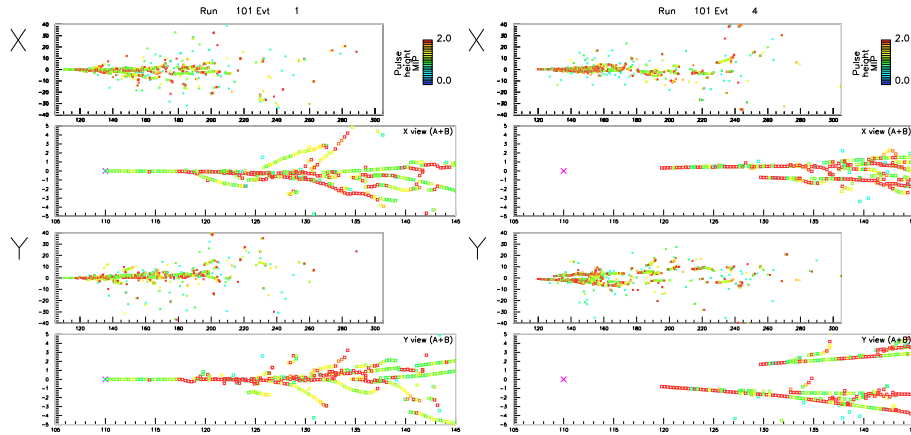
Figure 1.2: Full GEANT3 simulation of a 1.5 GeV single electron (left) and π^0 (right) as detected in a liquid argon detector. Events are shown in windows 40 cm wide and 200 cm long, followed by a blow-up of the vertex region 10 cm × 30 cm. The particle origin is shown with the pink cross. Color scheme of the digitizations is adjusted such that a green "hit" indicates a single MIP whereas a red "hit" indicates an energy deposit of two or more MIPS. It is important to notice that a 'tip' of a converting photos is red for a few cm indicating a presence if two overlapping particles.

reducing the systematic uncertainties. Corrections based on the event and detector simulations will be very small and therefore not very much affected by a relatively poor knowledge of the low energy neutrino physics.

1.4   Particle Identification and Energy Resolution of The Liquid Argon Detector

Imaging nature of the liquid argon detector combined with a very precise measurement of the ionization density dE/dx allows very efficient an unambiguous identification of stopping particles. Observation of the development of the electromagnetic cascade with very high spatial granularity differentiates between 'electromagnetic' and 'non-electromagnetic' objects with high efficiency, which we assume to be 100%. The key to the ν_e appearance experiment is very efficient e/π^0 separation. Fig.1.2 illustrates some of the the basic features of the electron and π^0 events recorded in the liquid agon detector.

The π^0-induced background occurs in two distinct categories of interactions:

- (A) events with one or more charged particles produced at the interaction points. These particles will define the interaction point with an accuracy

of $few\ mm$.

- (B) events no no charged particles produced alongside π^0. A coherent production of π^0's off nuclei is a good example of such events

Even ignoring the transverse shower information one can achieve a rejection factor of π^0's vs single electrons of the order of 40 by demanding that the ionization density over the first 2 cm of the track is consistent with a single track. Such a cut will reject about 10% of early showering electrons. For events in category (A) an additional rejection factor of 15 is accomplished by a requirement that the electromagnetic shower starts within 2 cm of the event vertex.

These two cuts are sufficient to reduce the number of π^0-induced background well below that of the intrinsic ν_e component of the beam. It is important to stress that there are many additional rejection factors which more difficult to quantify without a complete reconstruction of the events and which will provide redundancy and systematic checks of the background rejection procedure. They include:

- neutral current events, with outgoing neutrino, will have a significant p_t imbalance with respect to the incoming beam direction.

- distinct conversion points of two separate photons will be often visible. Owing to an excellent energy resolution an invariant mass of the π^0 can be reconstructed.

In th following we will, therefore, assume that the electron identification a the level of 90% with a π^0-induced background negligible with respect to the intrinsic ν_e component of the beam can be attained.

The liquid argon detector is, at the same time, a total absorption calorimeter and has a very good energy resolution. Electromagnetic shower energy can be measured with a resolution better that 1%. Stopping hadrons will have their energy determined to a few %, whereas an energy of an hadron-initiated cascade will be measured with an typical accuracy $\Delta E/E = 0.35/\sqrt{E}$. Implications for the accuracy of determination of the initial neutrino energy are less obvious: the energy resolution of the total observed charge as a measure of the incoming energy is limited by nuclear absorption effects and by kinematical factors like rest masses of the produced particles. It is of great help, in the energy regime of interest, that owing to a relative simplicity of the neutrino interactions all of the final state particles can be detected and their rest mass included in the neutrino energy determination. With this correction the incoming neutrino energy can be reconstructed with an accuracy $\Delta E/E \sim 10\%$. For some selected categories of events (like quasi-elastic scattering with lepton + proton in a final state) the neutrino energy resolution of the order of $1 - 2\%$ can be achieved.

	Neutrino	Antineutrino
Number of ν_μ CC events, no osc.	18,906	5,714
Background	56	23
Signal ($P_{osc} = 0.05$)	527	158
P_{limit} (3σ)	0.002	0.004
P_{limit} ($90\%\ CL$)	0.0012	0.0025

Table 1.1: Event rates and attainable limits on the oscillation probability for 5 years run of 50 kton detector with medium energy NuMI beam and $4 \times 10^{20} POT/year$.

1.5 Physics Potential of The Liquid Argon Detector

Physics potential of a specific off-axis experiment depends somewhat on the detector location. We have not performed the optimization process, yet but we use as an example a 50 kton detector located at the distance of 820 km from Fermilab and 11 km off-axis. We assume that 85% of the detector volume will be used in the experiment. We will assume that the efficiency to identify the ν_e CC interaction is 90% and that the background is dominated by the intrinsic ν_e component of the beam, which is well constrained by measurements at the near detector.

The experiment will measure the probability of $\nu_\mu \rightarrow \nu_e$ transition. The expected signal and background rates as well as the sensitivity of the experiment is summarized in Table.1.1.

Comparison of the attainable levels of probability with the Fig.1.1 gives an indication of the sensitivity of the experiment in terms of the physically interesting parameters: mixing angle, mass hierarchy and and CP phase δ. It is quite obvious that there is no unambiguous answer to a question: what is the sensitivity of the experiment to the $\sin^2 2\theta_{13}$?

The ultimate sensitivity can be achieved with the increased NuMI beam intensity with the proposed Proton Driver. Fig.1.3 shows the expected significance of the observed excess of the ν_e CC events for different mixing angles and for different mass hierarchies, for different mixing angles and for different values of the CP phase. It shows that the ultimate off-axis experiment can reach several standard deviations discovery even in the physics scenarios beyond the reach of the proposed reactor experiments.

1.6 Program of the Neutrino Oscillation Studies with FLARE at NuMI

A liquid argon detector in a nominal NuMI beam will enable a sensitive measurement of the $\nu_\mu \rightarrow \nu_e$ transition probability for neutrino and antineutrino
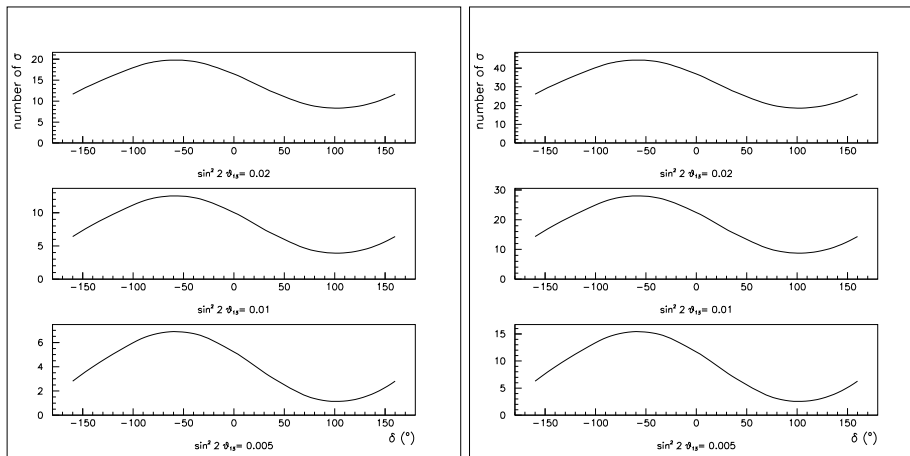
Figure 1.3: Significance of the observed excess of ν_e CC events in 6 years run of a 50 kton liquid argon detector in the NuMI beam enhanced with the Proton Driver as a function of the CP phase δ for different mixing angles θ_{13}. Left graph is for the inverted hierarchy, right one for the normal hierarchy[43].

beam.

Can such a single experiment provide an unique answer to all the questions mentioned earlier? What will be required to sort out possible ambiguities in the interpretation of the experimental results in terms of physically interesting parameters? We cannot answer these questions now, but we argue that the proposed detector offers a long range scientific program aiming at the ultimate determination of the parameters of the neutrino oscillations.

Fig.1.1 shows that possible results consistent with the oscillation interpretation lie in two bands corresponding to two possible neutrino mass hierarchies: normal (blue ellipses) and inverted (red ellipses). These bands are well separated, in bi-probability space, when the mixing angles is relatively large and they merge when the mixing angle is small.

There four possible classes out outcomes of the off-axis experiments and we will examine them in turns and we will argue that a liquid argon detector offers the best experimental possibility in each case:

1. the resulting P_ν and $P_{\bar\nu}$ lie outside the region expected in the oscillation scenario.

   Such an unexpected result would not be the first failure of the theoretical expectations. It would indicate that 'something else' is happening. The purity of the sample and the completeness of the event information offered by the liquid argon detector might be of crucial importance in establishing

what is going on.

2. the result is at one of the outer edges of the physics region.

   This would be very kind of the Nature. In such a case the mass hierarchy is clearly indicated, maximal CP violation is established, the CP phase is quite well known, mixing angle is well determined. The physics interpretation is unambiguous and the further increase of statistics will reduce the errors on the physics parameters. The advantage of the liquid argon detector here lies in its high detection efficiency, making it equivalent to much larger conventional detector or much brighter neutrino beam.

3. the result is somewhere in the middle of the allowed region, where two bands overlap.

   This may well be the most likely outcome. Depending on the exact location of the result there will be some level of ambiguities in the physics interpretation of the experimental results. We illustrate this case by taking an example of the possible result: let $P_\nu = 0.0167$ and $P_{\bar{\nu}} = 0.0173$. From Table.1.1 we find that they will be measured with the relative accuracy of 8% and 14% respectively after 10 year run in the nominal NuMI beam, or in one year exposure in the Proton Driver era. Fig.1.4(left) shows that there are four different combinations of physics parameters which are consistent with such a measurement. Further reduction of the statistical sharpness the allowed regions of phase space but it will not resolve the ambiguities.

   As the Fig.1.4 (right) shows even a precise measurement of the energy spectra of oscillated ν_e CC events does not help very much: they are nearly identical in all four cases for the NuMI beam conditions. The degeneracy can be broken and an unique interpretation can be achieved by combination of these results with the results of an experiment carried under different conditions. A longer baseline and accordingly bigger mass effects are of particular help. Fig.1.5(left) shows an example of the ν_e CC events detected in a NuMI-like low energy beam aimed at the NuMI off-axis detector from Brookhaven for the four, previously ambiguous physics scenarios. Ambiguities will be resolved and the parameters neutrino oscillation parameters determined with the accuracy given by he available statistics. Fig.1.5 (right) shows that the NuMI/BNL beam combination is a very powerful tool to determine the mass hierarchy. The observed rate of ν_e appearance are different because of difference in the matter effects which, in turn, depend on the mass hierarchy.

   In this particular case the advantage of the liquid argon detector, beyond the usual efficiency argument, is its isotropy of the good detection efficiency. This is important as the BNL beam comes from considerably different direction and a conventional planar detector would not be quite optimal. A good energy resolution with no long tails of the resolution function and very good rejection of π^0-induced background is very important for the wide-band BNL beam.
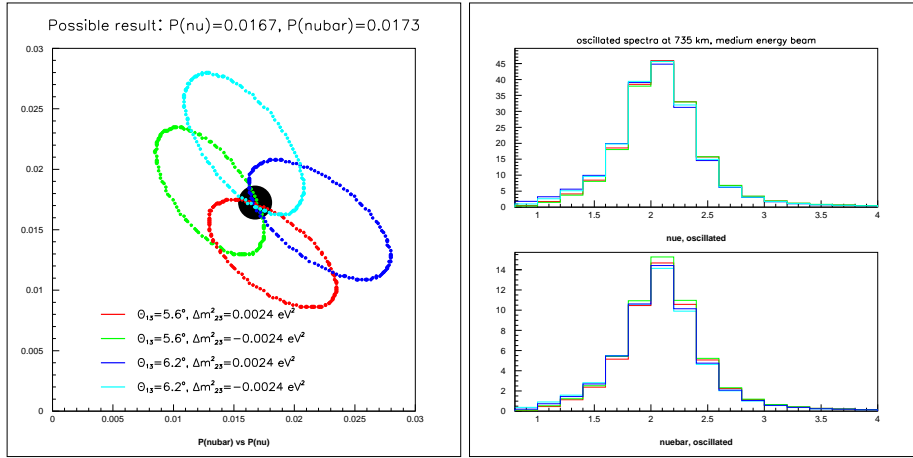
Figure 1.4: Left: Values of P_ν and $P_{\bar{\nu}}$ expected for different values of the CP phase δ and two mixing angles for both mass hierarchies. Right: Spectra of ν_e CC events produced in four different physics scenarios consistent with the selected values of P_ν and $P_{\bar{\nu}}$. Colors of histograms correspond to the sets of parameters indicated on the left graph. Top graph is the neutrino beam case, bottom is the antineutrino beam case.

4. the experimental result is in vicinity of the origin of the coordinate system

   A very small or none signal of ν_e appearance signal is detected. The mixing angle $\sin^2 2\theta_{13}$ is shown to be very small or a very tight limit is set. There is no information on the mass hierarchy, nor on the CP violation. In this case the limit obtained by a liquid argon detector is equivalent to that of six time larger conventional detector (or six times more intense neutrino beam), the reduction of background (relative to the conventional detector) contribution an additional factor of two.

   A null result of the several-year long appearance experiment would produce a very tight limit on the mixing angle, but it would be somewhat disappointing nevertheless given the scale of invested effort. It is therefore of great importance to examine other possible uses of such a detector.
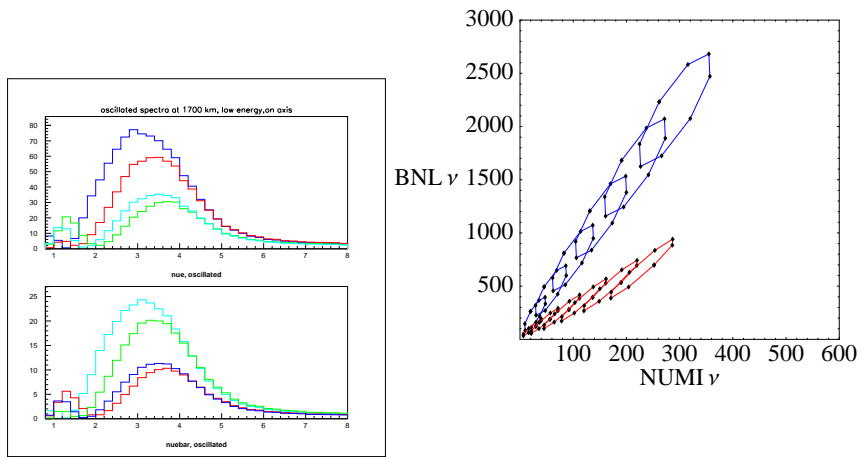
Figure 1.5: Left: Spectra of the ν_e CC events detected in the low energy beam produced at Brookhaven and directed towards an Off-axis liquid argon detector. Four different colors correspond to the four ambiguous (in the NuMI beam case) physics scenarios. Colors of histograms correspond to the physics parameters as in Fig.1.4. Right: comparison of the observed ν_e appearance rates in the NUMI and BNL beams. Different ellipses correspond to different values of the mixing angle[44].

Chapter 2

Physics Potential of a Surface Liquid Argon Detector

The primary motivation for an of-axis detector is the study of neutrino oscillations with the NuMI beam. Given the magnitude of the investment in the detector on one hand and a possibility or relatively un-eventful run if the mixing angle is very small it is very important to examine other possible physics topics which can be addressed with such a detector.

2.1 Free running surface detector operation

To study neutrino beam related interactions it is sufficient to record the waveforms of the wires signals in the time frames corresponding to the beam spill. The beam arrival time establishes the reference time for the measurement of the drift time. The duration of the neutrino extraction, 10 μsec introduces an error on the absolute position of the event of the order of 1.5 cm but this is inconsequential for the reconstruction of the interaction.

In order to be able to address other physics topics, like a search for rare phenomena, it is necessary to read out the detector continuously. This leads to several potential problems which are addressed in this chapter:

- large volume of data

- lack of the time reference, T_0

- cosmic rays induced backgrounds

It is important to point out that the data recorded in T300 module in Pavia were taken at the surface, thus they provide a very important check on the feasibility of the surface detectors.

2.1.1 Data rates and data acquisition

It is expected that the front-end electronics will provide a significant data reduction by performing cluster finding and baseline subtraction. The amount of data passed to the data acquisition system may contain some raw digitization in the region-of-interest (ROI) in the early stages of the experiment, but it is expected that after the initial debugging phase of the experiment only the 'hits' corresponding to the physical signals will be recorded. The data rates will be dominated by cosmic muons. Large electromagnetic showers or hadron-initiated cascades occur as well, but their rate makes them to contribute little to the average data rate. The effective area of the detector is of the order of $2,000\ m^2$ hence the average rate of cosmic muons is about $200\ kHz$. Majority of muons will range out in the upper part of the detector. Ranging out and angular distribution of the cosmic rays in conjunction with almost vertical wires geometry will lead to relatively small number of wires recording signals. To set a safe upper limit we assume that the average number of hit wires is less than 2000. Assuming 4 bytes per digitization it leads to the expected data rate of $1.6\ Gbytes/sec$, well within capabilities of a relatively modest data acquisition system comprised of few hundred of PC's.

While the instantenous data rate does not present a major problem, the overall data size is much more challenging: $100\ Tbytes/day$ and $30\ pbytes/year$. Data storage and analysis systems with such capabilities are likely to be relatively standard in the near future, but they will nevertheless require substantial investment.

It is very likely, however, that the data volume problem will be greatly reduced, by a factor of thousand or more. Vast majority of the data will be associated with cosmic muon tracks. They can be easily recognized by the data acquisition system and subsequently removed from the data stream. Even in the case where such data will be of physics interest it is very likely that a small fraction like 0.001 of them will be sufficient.

2.1.2 What is a T_0??

The distance of particle trajectory from the wire plane is determined by the drift distance, which is the difference of the arrival time and the 'production' time. The former is recorded by the electronics. The latter one is provided by th beam gate for the accelerator-oriented experiment. What is the T_0 for an object recorded asynchronously, like supernova neutrino.

In the large detector there will be several 'tracks' drifting the sensitive volumes at the same time, hence there is no global T_0 for an 'event' or a time frame. Instead, the reference time is a property of the 'object' in question. How can one determine what is the appropriate T_0 for a given set of digitizations forming a trajectory?

Before answering this question let's examine a consequence of applying an incorrect value of T_0 in the analysis of a given trajectory. Too early T_0 used will lead to an assignment of a too large of a distance from the wire plane to

the given track. If the track in question crosses the cathode plane then the points in vicinity of the cathode will be assigned unphysically large distance, thus indicating that the T_0 value used was incorrect. In a similar manner, if too late T_0 is used and the track crossed the wire plane it will b assigned negative distance. Tracks crossing the cathode plane or the wire plane do determine their own T_0.

Tracks segments fully contained within one drift volume will have a range of possible T_0 values. The correct one can be determined by using the observed ionization of delta electrons along the trajectory. The energy of the electrons can be determined from their range, which is translationally invariant, hence independent of the assumed T_0, hence the produced signal is known for them. The drift distance, and hence the T_0 for the object in question, can be determined from the measured signal corresponding to the delta ray as the attenuation is known from the continuously monitored electron lifetime.

2.2 Cosmic rays: background or signal?

High rate of cosmic muons leading to a huge data volume is likely to be a nuisance. Almost all of the can be easily recognized and discarded by the data acquisition system. This is a very likely scenario.

We should note, however that this detector will produce unprecedented volume and quality of data on the cosmic ray fluxes. Large area covered, high spatial resolution, good particle identification will provide a new window of the cosmic ray fluxes. Composition and spectra of cascades, correlations between electromagnetic and hadronic components, other correlations can be studied. It is not clear if such a dedicated experiment is worth the effort, but why not look at this data before throwing them away?.

2.3 Supernova Neutrinos and Physics Potential

The core collapse of a massive star is an abundant source of neutrinos and antineutrinos of all flavors, with energies in the tens of MeV range, and which are emitted over a timescale of tens of seconds. A core collapse neutrino signal was detected for SN1987A in the Large Magellanic Cloud, 55 kpc away, by the Kamiokande-II and IMB water Cherenkov detectors. Several neutrino detectors online now are sensitive [45].

The neutrinos from a core collapse in our Galaxy will bring a wealth of information. Note only will they illuminate the details of the core collapse mechanism via their time, flavor and energy structure, they will also provide a tremendously bright source for fundamental physics. Although the potential for kinematic mass limits (which for SN1987A were among the best at the time) is now exceeded by laboratory experiments, again the energy, flavor and time structure of the neutrino burst may provide information on fundamental neutrino parameters. For instance, flavor transitions in the stellar core due to

matter effects may occur, depending on the value of θ_{13}, and whether the neutrino mass hierarchy is normal or inverted can dramatically change the nature of the supernova signal. These signatures have been explored in several references [46, 47, 48]. The signatures are somewhat core collapse model-dependent, but there are some relatively robust features of the neutrino signal, on which one can base oscillation studies e.g. the hierarchy of energies for different flavors ($\bar{E}_{\nu_{\mu,\tau}} > \bar{E}_{\bar{\nu}_e} > \bar{E}_{\nu_e}$). Better understanding of the collapse mechanism via the neutrino signal feeds back to neutrino physics (and vice versa).

Supernova neutrino detectors require energy and direction sensitivity, and *good flavor sensitivity and tagging ability* is essential for extracting physics. Because the largest detectors currently online have a primary sensitivity to $\bar{\nu}_e$ via inverse beta decay, sensitivity to flavors other than $\bar{\nu}_e$ is especially valuable. In particular, because an interesting feature– a sharp burst of ν_e's, due to "shock breakout" – is expected near the onset of the signal, ν_e sensitivity is especially desirable.

Finally, there is the potential for an early alert to astronomers, since the photons associated with the disruption of the star (the supernova itself) will arrive later than the neutrino signal by hours or perhaps longer, dependent on the nature of the stellar envelope. For an early alert, pointing capability, i.e. sensitivity to neutrino interactions which preserve directional information, is highly desirable.

The expected frequency of stellar collapses in our galaxy is about one per thirty years, which is often enough to give one a reasonable hope of seeing one on the timescale of a large neutrino experiment, yet rare enough to motivate special care to extract maximum information from an event.

2.3.1   Supernova Neutrino Signal in Liquid Argon

The supernova neutrino signal in liquid argon has been studied in some detail in references [46, 47, 48], in the context of an underground detector. There are three main classes of relevant neutrino interactions: elastic scattering, charged current, and neutral current.

- Elastic Scattering

  Elastic scattering of neutrinos off atomic electrons,

$$\nu_x \ + \ e^- \ \rightarrow \ \nu_x \ + \ e^-, \tag{2.1}$$

  has both CC and NC components, and can provide pointing information. The signature in liquid argon is a single electron track.

- Charged Current Interactions

  Neutrinos and antineutrinos can interact via quasi-elastic charged current reactions with neutrons and protons in nuclei:

$$\nu_e \ +^{40} Ar \ \rightarrow \ e^- \ + \ ^{40}K^*, \tag{2.2}$$

Channel	Number of events at 10 kpc
Elastic scattering	665
Charged current ν_e	3120
Charged current $\bar{\nu}_e$	270
Neutral current ν_x	15220

Table 2.1: Numbers of supernova neutrino events expected in a 50 kt liquid argon detector.

with a threshold of 1.5 MeV and

$$\bar{\nu}_e \ +^{40} Ar \ \rightarrow \ e^+ \ + \ ^{40}Cl^*, \tag{2.3}$$

with a threshold of 7.48 MeV. At high energy, inelastic charged-current processes may yield neutrons or other particles as well; however, in the tens of MeV regime relevant for most of the supernova neutrino signal, the contribution is relatively small. CC interactions may be identified via the $e^{\pm}$ track, in coincidence with de-excitation gamma rays from the resulting nucleus.

- Neutral Current Interactions

  The neutral current excitation of argon,

$$\nu_x \ +^{40} Ar \ \rightarrow \ \nu_x \ +^{40} Ar^*, \tag{2.4}$$

  for both neutrinos and antineutrinos, can be detected via its de-excitation gammas. Neutrons or other particles may also be produced at higher energies.

The number of interactions scales simply with mass, and as $1/\text{distance}^2$ Table 2.1, based on ref [48], shows expected numbers of events in a 50 kt detector for these channels, for a core collapse at 10 kpc, assuming no oscillation effects.

The relative numbers of events in each channel may change dramatically due to flavor transitions in the stellar core, depending on the values of neutrino mixing parameters. If one assumes that these channels can be tagged effectively, and the parameters are favorable, one may have sensitivity to both θ_{13} and the mass hierarchy. References [46, 47, 48] explores in some detail these possibilities: the main conclusions [48] are: if θ_{13} is large enough ($> 3 \times 10^{-4}$), one may distiguish inverted from normal hierarchy; for $\theta_{13} < 2 \times 10^{-6}$, liquid argon may set an upper limit on θ_{13}; and for θ_{13} between these extremes, it may be possible to measure it with liquid argon, even in a several kton scale detector. However, the supernova parameters are important to the sensitivity to mixing: if the spectra of ν_e, $\bar{\nu}_e$ and $\nu_{\mu,\tau}$ neutrinos do not differ sufficiently, then one may not be able to measure θ_{13} or distinguish normal from inverted hierarchy, and larger scale ($\sim$100 ton) detectors may be needed.

However, in combination with other detectors (which may constrain both oscillation parameters and the supernova physics) and perhaps with partial knowledge of some of the parameters from e.g. long baseline experiments, a liquid argon detector, with its excellent multi-flavor capability, may yield significant constraints.

2.3.2 Backgrounds

The expected instantenous event rates from a nearby Supernova can be high nevertheless the expected backgrounds must be considered very carefully. The $200 \, kHz$ of cosmic muons is not a major problem per se: a small tube surrounding every incoming cosmic ray particle (or shower initiated buy it) can be easily removed from the fiducial with a minimal loss of the signal rate thanks to very high spatial granularity of the detector.

The dominant potential problem may be caused by the muon spallation and muon capture products, an example being ^{40}Cl with a lifetime of 100 sec. All the muons stopping inside the detector volume are detected and the volumes containing potential capture products can be excluded from the analysis. The size of the excluded region must include the diffusion and the accuracy with which a position of the end-point is known as a function of time, as a result of the fluid movement. The latter effect dominates as the velocity of the liquid circulation reaches up to $v = 7 \, cm/sec$ thus giving up to $10 \, m$ displacements. The liquid circulation is laminar and it is, in principle, well known. In practice a dedicated measurement system will be necessary to validate the predictions and to keep the loss of the useful fiducial volume to the acceptable level.

A careful analysis of cosmogenically produced backgrounds as well as the backgrounds produced by incoming neutrons (the latter confined to the upper parts of the detector) is necessary to evaluate the real potential of the surface detector.

2.4 Proton decay

The question of nucleon stability is of fundamental importance and it has received a great deal of attention the past few decades with large water Cherenkovs in the forefront, but even a relatively small fine grained calorimeter, Soudan 2, making a significant contribution.

A 50 kton liquid argon detector would represent about two orders of magnitude step over Soudan 2, at the same time providing more detailed information about the detail of a possible nucleon candidates.

2.4.1 Motivation and Signatures

A 50 kton water Cherenkov detector of the SuperK is running since several years and its limits on the proton lifetime keep improving with time. Further major improvements requires a significant increase of the detector mass, perhaps to the

level of Mton or so. This is true for all of the decay modes where the efficiency of the water Cherenkov is very high and this includes decay modes involving electrons and muons.

A niche for other detector technologies exists if proton decays primarily into K mesons. Kaons at these energies are below the Cherenkov threshold in water, hence the the SuperK detection efficiency is relatively low and the backgrounds are significant , as only secondary or tertiary particles are detectable.

A $p \rightarrow K^+ + \nu$ decay has been advertised for a long time as primary example of the analyzing power of an imaging detector like a liquid argon TPC. Fig.2.1 shows an example of a 0.5 GeV charged kaon as detected in the detector. The identification is unambiguous and heavily over-constrained: kaon is identified by its decay chain $K^+ \rightarrow \mu^+ \rightarrow e^+$. Kaon track is characterized by large ionization density, increasing towards the end point. Muon track has well defined, and well measured but the range, momentum and it has corresponding ionization density. An electron from the muon decay is easily identified and well measured. The entire event occupies a relatively small volume of the detector, approximately a cube $0.5 \times 0.5 \times 0.5$ m^3. Not all instances of the kaon decays are equally spectacular, some kaons decay at rest, some interact before the decay. Nevertheless, as the ICARUS studies have shown the efficiency for the detection and identification of the $p \rightarrow K^+ + \nu$ decay in the liquid argon detector exceeds 90%.

2.4.2 Backgrounds

It is widely assumed that the nucleon decay search requires detectors to be placed in deep underground laboratories. There are two reasons for that:

- to reduce the rate of particles, mostly muons, crossing a very large volume of the detector to the levels allowing reliable particle detection and reconstruction.

- to reduce the rate of cosmic rays induced backgrounds, especially those induced by neutrons

The first concern is clearly dependent on the detector technology. A detector with good three-dimensional granularity, with no space charge effects can easily be operated on the surface and evidenced by the T300 module operation in Pavia. The nuisance of dealing with huge data rates it he primary cost.

Far more important concerns is that of cosmics-induced backgrounds. The majority of cosmic rays are muons. They, or any spallation products induced by them, do not constitute a significant background sources as the energies expected for the proton decay products are very large, in hundreds of MeV range.

A serious concern is a neutron-induced background. After all, neutron rates is only a factor 100 smaller than the muon rate. It is very unlikely that a search for $p \rightarrow e^+ + \pi^0$ can be conducted on the surface, for example. The decay modes involving kaons are different: the signal consists of a single charged kaon in
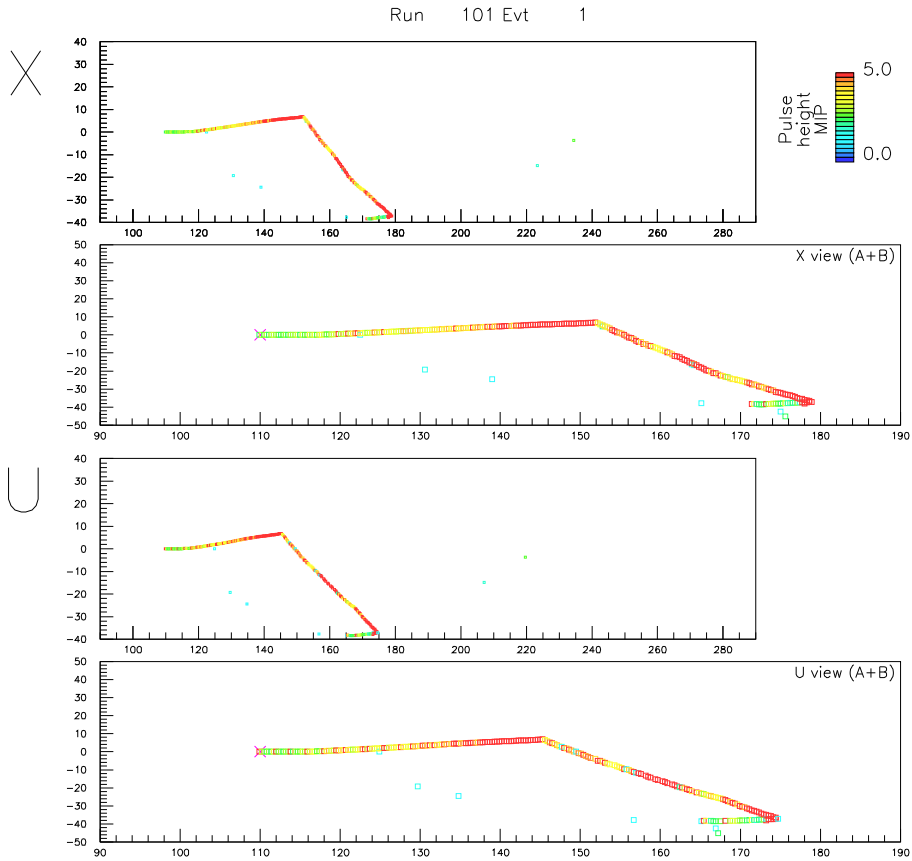
Figure 2.1: 0.5 GeV K^+ as detected in th liquid argon TPC. The color scale is adjusted such, that red corresponds to the ionization density equivalent to 5 minimum ionizing particle.

the middle of a large detector. Strangeness conservation in strong interactions guarantees absence of such a background induced by neutrons. To maintain good sensitivity to proton decay it is important that the background levels are kept below one event per year or so. The required rejection rate is huge and most unlikely processes can easily swamp the measurement. An example of a possible background could be a neutron-induced associated production of $\Lambda + K$ with Λ escaping a detection. It has been demonstrated that this background does not require a very deep laboratory and the shallow depth of WIPP is adequate to provide a background-free measurement[49] even without invoking any sophisticated analysis. An analysis of the surface detector requires far more work, and the ultimate result depends on the quantitative estimate of the

probability of the produced Λ escaping detection. Given a very low detection threshold in the liquid argon the expected rejection factor will be very large, but it is not known at the present time.

Even if the neutron-induced background is found to be negligible one needs to worry about K^0 component of the cosmic rays, as they can produce a single charged kaon in a charge-exchange reaction.

A significant background rejection factor against the background induced by the hadronic component of the cosmic rays will be offered by the size and the analyzing power of the detector. It is very likely that the majority of neutrons and K^0 are produced in showering events and the accompanying particles will be detected in the detector. A flux of 'isolated' hadrons is probably much smaller.

The last line of defense could be a use of the top layer of the detector as a hadron absorber. It would reduce the effective fiducial volume, but it could still offer a significant improvement of the available limits or provide a discovery opportunity. It is important to point out that this upper region of the detector will provide a very good measurement of the actual backgrounds, hence a defense of a possible positive result of the search would be relatively easy.

Given the magnitude of the necessary rejection factor against the cosmic rays background a very detailed analysis of the performance of the proposed detector on one hand and the available data on the hadronic component of the cosmic rays on the other hand is necessary to evaluate reliably the physics potential of the surface detector.

Chapter 3

Small Liquid Argon Detectors in the Intense Neutrino Beams

Fermilab is blessed with two intense neutrino beams, the second one nearing its completion. Unprecedented beam intensities offer very high interaction rates even with modest size detectors, at the scale of 40 tons. Liquid argon TPC is a particularly suitable detector for the experiments in the near halls of Mini-BOONE and NuMI beams. Simple topology/low multiplicity of the neutrino interactions at these energies in conjunctions with good particle identification and good energy resolution will permit complete kinematical reconstruction of the final states. Very low threshold of particles detection, few MeV for hadrons and sub-MeV for electrons, may be the deciding factor for several physics measurements. Relatively high density of liquid argon offers a good stopping power hence maximizing the size of the useful fiducial volume.

Small detectors should be relatively simple to construct and operate as a scaled down versions of the ICARUS modules, whereas their size will eliminate or greatly reduce logistics and safety concerns.

3.1   Beam Spectrum and Beam Composition

NuMI neutrino oscillation experiments aim at very precise determination of the oscillation parameters. In a longer run they will become systematically limited by the understanding of the neutrino beam spectrum and its composition. Understanding of the ν_e component of the beam is important for the appearance experiments.

The un-oscillated beam and its composition can be measured at a near detector position. A reliable ν_e measurement is difficult there, as the background from π^0-containing NC and ν_μ CC events is very high and very different from

the far detector. High rejection power of NC vs CC events and electrons vs π^0's, related to very high spatial granularity of the detector, makes the liquid argon TPC especially well suited for this purpose.

Neutrino beam spectrum reconstruction requires good energy resolution and symmetric resolution functions. Absence of long tails of the resolution function is especially important in the regions where the energy spectrum is changing very rapidly. At low energies good neutrino energy calibration and resolution is limited by kinematical effects of rest masses and by the difference in response for different particles species. Low detection threshold and good particle ID minimize these problems in case of a liquid argon detector.

3.2 Neutrino Scattering Physics at Low Energies

Experimental neutrino physics was in its infancy when low energy beams were operational: beam intensities were very, very low, fluxes were known very poorly, detectors were very crude or, in case of bubble chambers, small and labor intensive. The world sample of events are in the hundreds for some exclusive channels and in the tens of events for other channels. As a result, our knowledge of neutrino interactions, even the total cross section, in this energy regime is particularly poor.

The relatively low energies of current accelerator neutrino beams (.1-20 GeV range) span the region below which the single pion production cross section turns on, and above this, where deep inelastic scattering (DIS) turns on. With two neutrino beamlines at Fermilab which span this rich energy range, and precision neutrino detectors, a host of interesting physics can be addressed.

The difference in the neutrino fluxes on these two beamlines translates to the breadth of physics that can be covered with programs on both beamlines. The Booster neutrino beamline's low energy flux accesses low Q^2 interactions with a clean beam, free from DIS and neutron backgrounds from high energy neutrino interactions around the detectors. The NuMI beam flux spans the interesting resonance to DIS region with neutrino interactions up to 20 GeV. Some of the wealth of physics topics using these beams are described below.

3.2.1 Neutrino Physics at NuMI Energies

Neutrino Scattering in the NuMI beam spans the interesting transition region from single pion production to deep inelastic scattering. Onset of strange and charm particles production is taking place there too. This is the place where limits of applicability of perturbative QCD may be studied.

Large samples of several millions of well reconstructed neutrino events, with complete kinematical reconstruction of well identified particles will be a veritable mine of bread and butter physics, especially because the forthcoming measurements of particle production (MIPP) will enable neutrino flux prediction at the level of few percent.

A typical laundry list of physics topics includes, but is not limited to:

1. Total ν_μ and $\bar{\nu}_\mu$ Cross-sections -vs- E_ν notably below 20 GeV

2. ν_μ and $\bar{\nu}_\mu$ Quasi-elastic cross-section

3. ν_μ and $\bar{\nu}_\mu$ resonance processes

4. Differential cross-sections, structure functions, and studies of PQCD and Non-PQCD; notably what is DIS and how does it link with non-scaling processes, such as QE and resonance

5. Cross-section of exclusive processes such as charm and strange particle production

Nuclear effects in neutrino interaction can be measured by using sheets of targets -from carbon to iron to lead - in the upstream end of the experiment liquid argon detector.

While these physics topics are interesting in their own right they are also of great importance for the precise determination of of the oscillation parameters.

3.2.2 Neutrino Physics at Booster Energies

The Booster neutrino beam provides high intensity neutrino beam with energies below DIS turn-on. A liquid argon time projection chamber used to detect neutrino interactions in this beam can offer precision measurements of cross sections as a function of Q^2, especially in low Q^2 regime, thus allowing for determination of form factors and study of nuclear effects.

High intensity beams allow for study of low rate cross sections, such as ν_e-$e$elastic scatters, rich in interesting physics. A very important property of the LArTPC is a very low energy threshold for electrons. With low noise electronics and using the beam gate timing it will be possible to detect electrons with energies as low as 105 keV. In conjunction with low energy and high rate of the MiniBOONE beam this make such a detector particularly well suited for studies ν_e-e elastic scattering and a measurement of the neutrino magnetic moment. We estimate that an experiment using a 100 ton detector can improve the existing limits by more than an order of magnitude.

Listed below are examples of the physics topics available for study on this beamline.

1. Low Q^2 form factor measurements, in particular, a measurement of the axial form factor and extraction of the strange part of the axial form factor

2. ν_μ and$\bar{\nu}_\mu$ Precision measurement of resonant and coherent single pion channels

3. Study of nuclear effects in $numu$ and $\bar{\nu}_\mu$ cross-sections at low Q^2

4. Search for non-zero neutrino magnetic moment using ν_e-e elastic scattering

3.3 Weak Mixing Angle

Measurements of the weak mixing angle in the neutrino sector were among the first experimental indications of the correctness of the electroweak model which later advanced to the rank of the Standard Model. The same kind of measurements started to cast some shadow on the this model or perhaps herald an arrival of The New Physics[54]. Liquid argon TPC is particularly well suited for studies of the neutral currents owing to the very low detection threshold and excellent muon identification. Very intense neutrino beams and good electron-π^0 separation offers an interesting opportunity of the study of purely leptonic reaction: $\nu_\mu - e$ scattering. It is not quite clear if the systematics can be controlled to the level required to measure the weak mixing angle with the precision comparable to NuTeV, but a low energy measurement may be interesting anyway.

3.4 Testing Ground For Neutrino Event Generators

Neutrino oscillation experiments make heavy use of Monte Carlo simulations to extract precise values of the oscillation parameters. Reliability of the extracted parameters starts to be limited by the reliability of the underlying event generators which, in turn, is limited by the scarcity of the experimental data.

Very large sample of well reconstructed low energy neutrino events will provide a stringent test for the neutrino event generators and will constrain various ad-hoc methods of linking exclusive channels with deep inelastic regime.

Complete solid angle coverage and particle identification and good energy resolution of the liquid argon detector will be of great asset here.

Chapter 4

Liquid Argon Imaging Technology

4.1   Brief History

The Liquid Argon Time Projection Chamber (LAr TPC), like many successful technologies, has several pioneers. Louis Alvarez experimented with a liquid argon incarnation of a bubble chamber[1] as early as the late sixties. Emerging technology of liquid argon based calorimetry has stimulated studies of production and collection of electrons in liquefied noble gases and in particular studies of drifting electrons over long distances in a liquid argon. Electron drift over several centimeters was demonstrated and the relation between electronegative impurities (oxygen) and the drift distance was quantitatively established in 1976[2].

First application of the liquid argon tracking detector to neutrino experiments was proposed in 1976 by Herb Chen [3] as a Fermilab proposal (P-496). This group demonstrated experimentally the drifting of electrons in liquid argon over distances of 30 cm [4]. The subsequent R&D effort at Irvine, Caltech and Fermilab [5] has lead to a program of developing working prototypes of these Time Projection Chambers.

These liquid argon imaging detectors require low noise front end electronics. Veljko Radeka, following a suggestion from Bill Willis, started working in this area in 1975. Consequently, the basic concepts of electrode geometry and signal processing for a time projection liquid argon ionization chamber were developed [6].

A decisive step in the development of the liquid argon imaging technology was a proposal by Carlo Rubbia [7] leading to the formation of the ICARUS project. Studies of electrons drifting over large distances in solid and liquid argon [9, 10], construction and operation of a collection of time projection chambers with increasing mass [11, 12, 13, 14, 15, 16] and experimental studies of scintillation and Cherenkov light emission in liquid argon [17, 18] were com-

pleted as part of the R&D efforts for ICARUS. This work is complemented by systematic studies of factors affecting the electron production and lifetime in Argon [19, 20] as well as by a design of front-end electronics and data analysis techniques [21, 22, 23] again, developed by ICARUS. A major step was the application of industrial filters used in the purification process [24] along with the demonstration of feasibility of liquid phase purification [25]. This progress has led to electron lifetimes of several milliseconds, even in very large detectors [26].

The Liquid argon Time Projection Chamber is a well established and mature technology. The ICARUS experiment is the first example of its application [27]. A successful design, construction and operation of a large 600 ton module [28] and the initial results of the collected data [29, 30] is a convincing demonstration of the maturity of this technology.

Another contribution to the liquid argon imaging detector technology has been a construction and successful operation of The Big liquid ARgon Spectrometer, BARS [33]. This detector constructed for the tagged neutrino beam at Serpukhov is a testimony to the fact that detectors are usually easier to construct than neutrino beams.

4.2   Principle of Detection Technique

The following description of the detection technology and its practical implementation is based on the ICARUS experience with the T600 module in Pavia. It is only a review of a small subset of the available information, judged to be the most relevant to the experiments discussed in this letter.

The analyzing power of the detector is well illustrated in Fig.4.1. Its salient features are:

- All charged particles produced are detected. The detection threshold is 0.2 Mev kinetic energy (for electrons). Two track resolution is on the order of a few mm.

- The three-dimensional view of the event is recorded with a voxel size on the order $3 \times 3 \times 0.5$ mm^3.

- Ionization, dE/dx, is measured locally with an accuracy on the order of 10%. It allows for good particle identification.

- Photon conversions are easily detectable with measurable energies. Radiation length in liquid argon is 14 cm (18 cm for photons)

- Energy resolution for stopping particles is very good. Energy resolution for electromagnetic showers is on the order of $\Delta E/E \sim 0.01/\sqrt{(E)}$; for hadronic showers it is on the order of $\Delta E/E \sim 0.2/\sqrt{(E)}$

A charged particle traversing the liquid argon produces electron-ion pairs. The number of ionization electrons produced per unit length of the track depends on the operating voltage. For typical operating conditions at 500 V/cm,
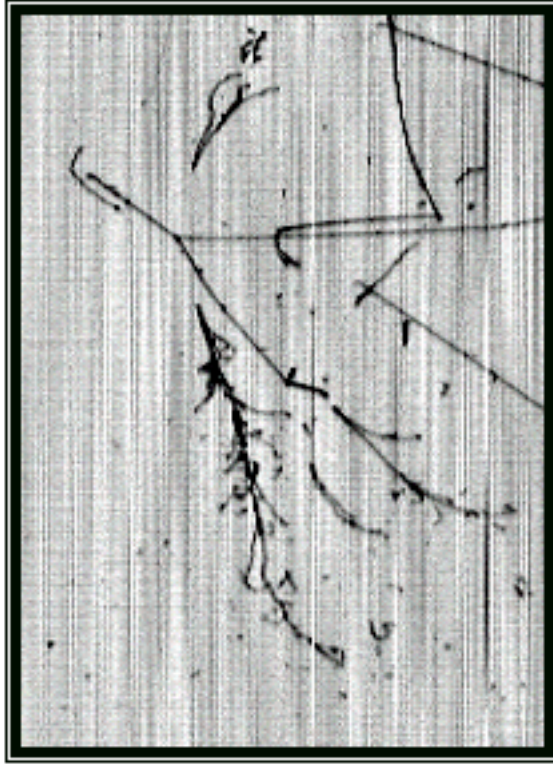
Figure 4.1: Hadronic event registered in the T600 module of ICARUS. The detector was operated in Pavia.

the number produce, $dQ/dx \sim 55000e/cm$ see Fig.4.2. A uniform electric field throughout the detector volume guides the electrons to collection electrodes. The drift velocity of these electrons depends on the electric field strength, Fig.4.3 typically 1.5 $mm/\mu sec$. This field strength leads to relatively long drift times up to 2 msec for 3 m drift distances. This, in turn, will set the requirements on the purity of the argon.

From the measured drift time, the particle distance from the collection wire can be determined, thus giving a two-dimensional projection of the event, as shown in Fig.4.1. In gaseous TPC's the position of the particle along the wire direction is provided by the signal induced by the avalanche on the the set of pads positioned behind the collection wire. Absence of an avalanche in liquid argon makes this technique unworkable here. Instead, a wire grid (or grids), placed in front of the collection wires, readout the signal induced by the passing electrons. With proper biasing these grids can be made transparent to the

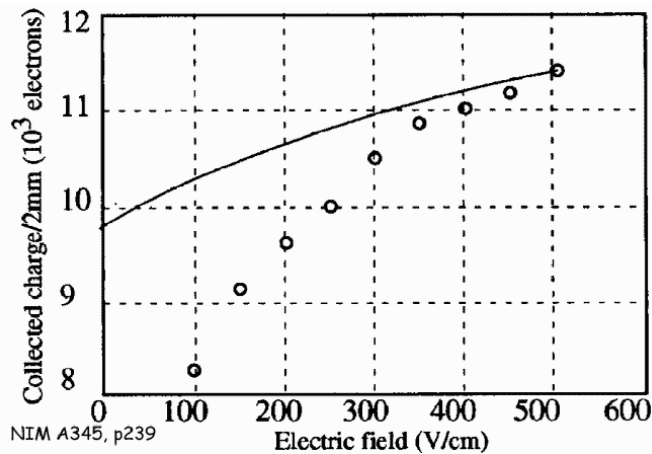Figure 4.2: Number of electrons collected per 2 mm of a minimum ionizing track [14]. Open circles represent data, solid line represents the variation expected from a simple Onsager recombination model.

drifting electrons and thus not attenuate the signal to be recorded on the collection wire[8]. This technique permits more than one additional coordinate to be obtained and provides redundancy for three dimensional reconstruction.

4.3 ICARUS T600 Module

The ICARUS T600 module is a dual 300 ton detector constructed as proof-of-principle, demonstrating the viability of a large scale liquid argon detector. Its design is tailored to the requirements of the underground experiment in the Gran Sasso laboratory. In particular, the rectangular module, designed with thin thermal insulation, can be constructed elsewhere, transported over the public highways to the laboratory, and is sized to fit through the laboratory's entrance gate.

The successful construction and operation of the T600 module is the primary evidence of the maturity of the technology. A large fraction of the technical solutions learned in building the T600 are directly applicable to detectors of different scale, both larger and smaller. However, some aspects, particularly those related to the cryostat construction and the cryogenic systems, are specific to the Gran Sasso experiment. We will mention them very briefly here.

4.3.1 Cryostat and Cryogenics

The design of the cryostat and the cryogenic system for the T600 is driven by the requirement that the LAr container have to be transported through the Italian
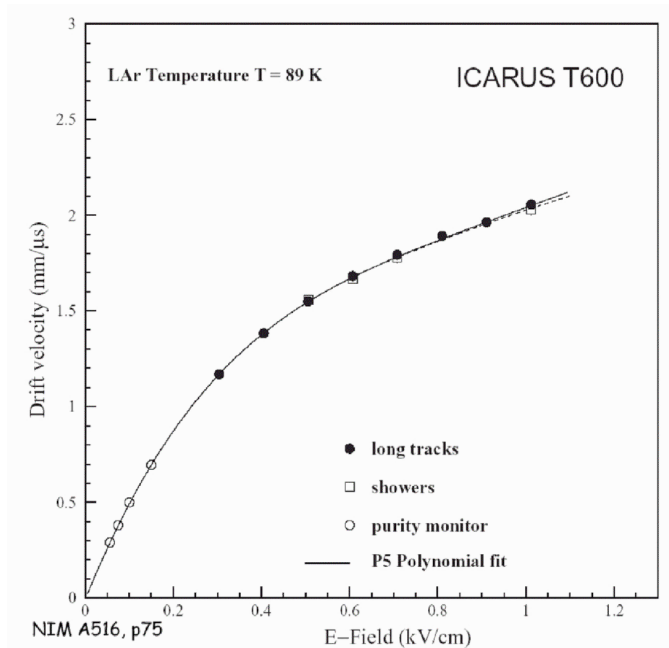
Figure 4.3: Electron drift velocity as a function of the electric field in the drift volume [26].

highways and to pass through the entrance gate of the underground Gran Sasso Laboratory [28].

Aluminum containers $4.2 \times 3.9 \times 19.9 \; m^3$ are built out of perforated aluminum honeycomb panels with embedded liquid nitrogen cooling pipes, sandwiched between aluminum skins. Thermal insulation is achieved through two layers of $20cm$ thick Nomex honeycomb structures on both sides of a perforated aluminum cold shield.

The cooling system is designed to keep the liquid argon temperature stable to 1° C over the entire detector volume. It is based on circulation of liquid nitrogen pressurized to 2.7 bar with a rate of 8 ton/hour/container.

4.3.2 Argon Purification

High argon purity is a fundamental pre-condition of the functional detector. For drift distances on the order of $2-3$ meters it is necessary to maintain an electron lifetime of several milliseconds in argon and this, in turn, requires that contamination of electronegative impurities be maintained at the level of 10^{-10} O_2 equivalent.

Purification of liquid argon from an initial purity level of about 1 ppm to the level of 0.1 *ppb* can be achieved by recirculation of the argon through a

combination of commercial filters: Hydrosorb and Oxisorb [24].

The T600 module is instrumented with two gas recirculation systems with nominal capacity of 25 $m^3/hours/system$ and one liquid phase recirculation unit with capacity of 2.5 $m^2/hour$.

The purification filters are designed for gas phase purification. However, dedicated studies [25] have demonstrated that they perform well for liquid argon as well. In fact, liquid phase purification is much more efficient due to the fact that a larger mass of argon can be purified in the same amount of time. It has also been demonstrated that the purity level of the liquid is much higher – by a factor of 100 or more – that the original gas as a result of impurities freezing out at the cold surfaces of the liquid container.

The purity level of liquid argon is a result of interplay of several effects:

- removal of impurities by the purification system

- inflow of oxygen due to potential leaks

- out-gassing from warm surfaces in the gas phase of the container, primarily the cables

Analysis of the performance of the purification system [25, 26] indicates that the contribution from leaks to the impurity level was negligible while the purity level improving steadily as a result of the purification process (liquid phase mostly). Although the purity level achieved during the test run corresponded to an electron lifetime of about 2 $msec$ the observed purification rate indicates that the ultimate purity level would correspond to a lifetime of 13 $msec$ [26].

4.3.3 High Voltage

The high voltage system must produce a uniform electric field in the drift volume. The T600 configuration contains a cathode plane in the middle of the container with collection wires on each side of the container, thus giving a maximal drift distance of 1.5 m. The module is operated with a drift field of 500 V/cm, hence the central cathode runs at a voltage of 75 kV. With future applications in mind, a short successful test run was performed with the high voltage operating at 150 kV.

High voltage for the T600 is supplied by a commercial HV power supply made by Heinzinger. A novel design custom-made HV feed-through was designed and built for the specific geometry of the T600 module. This design can be easily applied to other cryostats too.

The uniformity of the electric field is assured by a field cage consisting of a set of rectangular frames constructed from stainless tubing and spaced by 5 cm along the drift direction. . The frames are biased to potential linearly decreasing with a distance from the central cathode with a resistor chain. Four independent resistors, 100 $M\Omega$ each, are employed at every step for redundancy. The resulting current drawn from the HV power supply is 1 mA.

4.3.4   Inner Detector

Electrons produced by charged tracks in the detector volume drift to the sides of the module volume and are detected by 3 planes of wire chambers. The first two planes – so called induction 1 and induction 2 – register signals induced by the electron cloud traversing the wire plane. The third plane – the collection plane – collects all of the electrons drifted to it. The position of the wires registering a signal in conjunction with the measured drift time gives two coordinates of the originating track. This along with the information from the two induction planes, oriented at stereo angles $+60^o$ and -60° with respect to the collection wires, thus provides three dimensional information. All three position measurements from a given track segment have the same timing information, thus facilitating the three dimensional track reconstruction. Wire spacing within each plane as well as the distance between the wire planes is 3 mm. The planes are biased by about 300 V with respect to neighboring planes.

The chief requirement of the design of wire chambers is to assure survivability of all the wires during the thermal cycle of the detector cool-down. The problem is somewhat complicated by a difference of the thermal expansion coefficients of different structural materials used in the construction (steel and aluminum). The chambers are constructed using 150 μ thick steel wires tensioned with 5 N (horizontal wires) or 12 N (stereo wires). Chambers are constructed in a modular fashion with wires cut, spooled and cleaned at remote laboratories, and later unwound and mounted inside the detector.

A very elaborate tensioning system sets the initial tension of the wires and compensates the tension increase due to thermal cycle. A thermal cycle of the entire system was tested using a smaller, 10 ton, ICARUS prototype. None of the 1900 wires broke or even reached their elastic limit [16].

Twisted-pair flat cables are used to carry the wire signals out of the cryostat to the front-end electronics located on top of the detector. All signal feedthroughs are therefore at room temperature.

4.3.5   Readout Electronics

Liquid argon time projection chamber readout consists of a digitized waveform for every wire. Given a drift velocity of $v_{drift} = 1.5 \ mm/\mu sec$, a sampling rate on the order of 2 MHz is sufficient for waveform digitization. Because the signal size small, of the order of 15,000 electrons, the most critical parameter of the readout electronics is input noise.

The analog stage of the electronics is a commercial 32 channel board CAEN V791. It consists of a 32 preamplifiers based on the analog BiCMOS chip, a 16:1 multiplexer and a 40 MHz 10 bit FADC. There are two versions of the V791 boards with different shaping times for the collection/first induction plane and for the second induction plane. The latter conditions a bipolar induced signal into a signal with very similar characteristics to the signals from two other planes.

The electronics noise is dominated by the input stage of the first amplifier

and it is proportional (with an offset of 500 electrons) to the capacitance of the detector. For a typical channel with a capacitance of 400 pF the signal-to-noise ratio exceeds a factor of five for a minimum ionizing track.

Full digitized waveforms for all wires make for a very large data volume. This data set can be reduced in the digital stage of the front-end electronics, V789 board, by a dedicated ASIC performing hit finding. The resulting data (reduced or not) are stored in 128kB VDRAM and eventually, if triggered, transferred to the data acquisition system.

4.3.6   T600 Operation in Pavia

The complete T600 detector module was commissioned and successfully operated for several months in Pavia. The main focus of this technical run was a checkout of the entire system including the cool-down of the cryostat, purification of the liquid argon, and check of the detector performance.

Over the course of the run, tens of thousands of selected cosmic ray events were recorded including those with long horizontal tracks [30] or high energy cascades. The collected data has provided yet another demonstration of the imaging capability of the liquid argon TPC. It has also demonstrated that the cosmic ray and environmental background in the surface detector can be separated from other interactions in the volume.

The analysis of the data provides a valuable feedback for the software development, and has produced the first physics results with this technology [29].

Chapter 5

Liquid Argon Off-axis Detector

The ICARUS collaboration has demonstrated fundamentals of the liquid argon imaging technology:

- large quantities of liquid argon can be purified using commercial filters to the levels permitting drift of electrons over several meters

- large area wire chambers can be constructed in a manner ensuring their survivability of the cool down process and their operation at liquid argon temperatures

- low noise electronics can be designed and constructed providing a signal-to-noise ratio for detector capacitances up to 400 pF

The ICARUS collaboration has also demonstrated that a large scale implementation of such a technology is possible even with demanding constraints of the underground laboratory. It is a testimony to the success of the ICARUS project that attempts to design detectors at much larger scale are made quite frequently in the framework of neutrino factories[34] and/or future large underground laboratories[35].

5.1 Overview

With the fundamental principles proven to be well understood the principal challenge of a design and construction of a very large detector is of the engineering nature and it reduces to a problem of a design of a safe, cost effective and practically realizable detector. It should be pointed out that a possible scheme could involve construction of a number of ICARUS-like modules. This is not a cost effective solution, though.

It has been recognized that the a large detector constructed inside a single cryogenic vessel represents much more attractive possibility[34]. In this chapter

we present a design of a possible detector using such a concept. This design utilizes maximally the solutions used in the construction of the ICARUS module. There are several possible improvements, which can be incorporated in the design once the necessary R&D is successfully completed. We describe these possible developments in Chapter 8.

In the following we demonstrate that it is possible to construct a cost-effective detector large detector using the existing technology. As an example we use take a 50 kton surface detector constructed in off-axis position in a NuMI neutrino beam. Many of the industrial aspects (tanks, cryogenics, liquid argon) were studied by G. Mullholand from Applied Cryogenics Technology for the LANNDD project[36].

5.2   Liquid argon tank and the cryogenics

Large cryogenic tanks are built by industry to store liquefied natural gas (LNG). Several vendors offer a large variety of tanks with volumes up to $200,000 \ m^3$. For example purposes in the following we use Chicago Bridge and Iron[37], but several other vendors exist.

It is interesting to note that the thermodynamics of storage of liquid argon is quite similar to that of liquefied methane. The boiling points of argon and methane are $87.3 \ K$ and $111.6 \ K$ respectively. The heat of vaporization per unit volume of both liquids is the same within $\sim 5\%$ therefore the volumetric boil-off rates will be comparable for the same thermal insulation. The main difference between the storage of liquid argon and that of liquid methane stems from the difference in their densities: the liquid argon tank need to withstand 3.3 times higher hydrostatic pressure.

The tank necessary to store 50 $kton$ of liquid argon has $35,000 \ m^3$ volume and it would be a cylindrical tank 30 m high with 40 m diameter. There are several possible designs of storage vessels[37]. The one suitable for our application is that of a double wall and double roof vessel illustrated in Fig.5.1

To ensure reliability of the tank at the cryogenic temperatures the inner vessel will be constructed from full penetration butt welded nickel steel plates (Fe9NI, A553, Type I). The outer vessel is constructed out mild steel. Thermal insulation is provided by 1.2 m thick layer of Perlite purged with dry nitrogen. This thermal insulation implies that the boil-off rate of liquid argon will be in the range of $0.05\% \ /day$ or 25 ton/day.

It is very important to stress that this kind of tank is not capable of taking any significant external loads and in particular it cannot be evacuated.

Such a tank is very similar to the tanks constructed for gas industry, hence the construction costs can be reliably estimated. CBI quotes an estimated cost of turnkey system (excluding external piping, pumps, refrigeration system, electrical, instrumentation and controls) is $11 M. This cost does not include penetrations required for High Voltage and signal feed-troughs but they are expected to be well within the accuracy of the quoted price, which is about 20%.
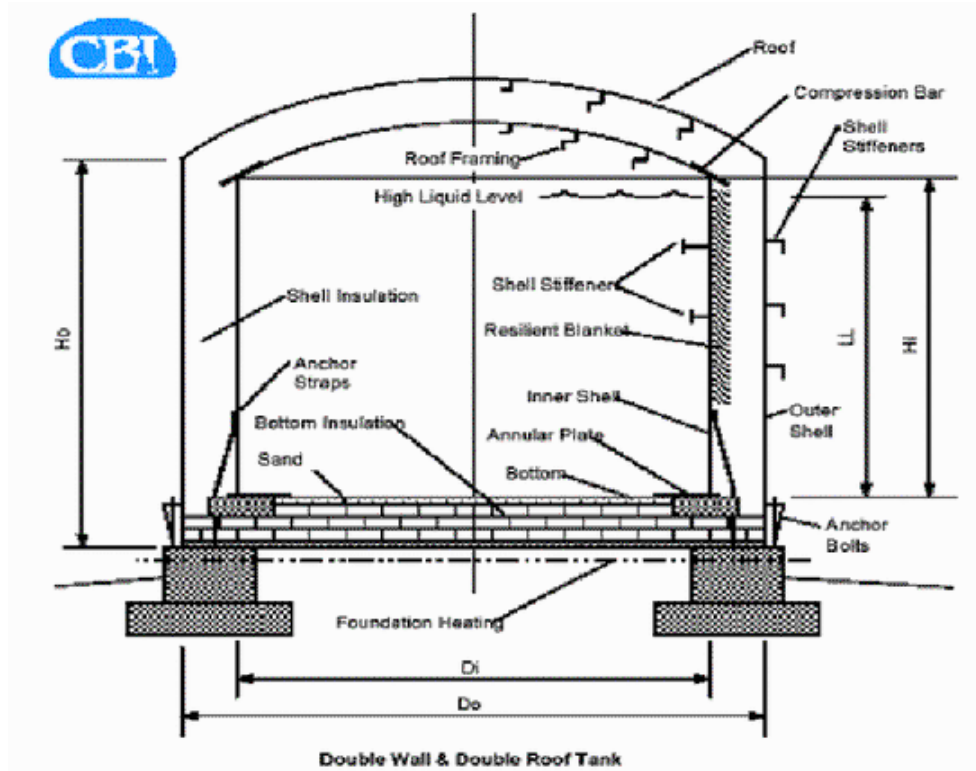
Figure 5.1: Double wall containment cryogenic vessel, CBI standard design

5.3   Liquid argon and the purification system

5.3.1   Liquid Argon

Liquid argon is a by-product of air liquefaction. It is widely used in industry for heat treatment, sintering or as a shield gas. An annual production of the liquid argon in the US is about $1,000$ *kton*. Specification of industrial grade liquid argon lists an oxygen content of 2 *ppm*, although in practice the purity levels routinely seems to be better than 1 *ppm*[38]. There exist grades of high purity, 0.1 ppm, of liquid argon but they do not present a cost effective avenue for a large experiment, especially that it may be difficult to maintain such a high purity level during the delivery and filling process.

The typical price of the liquid argon is of the order of $0.40/kg but the delivery costs may be quite significant. Following the study for the LANNDD[36] we use $0.60/kg as an estimated price for delivered liquid argon. This cost assumes

that the argon is delivered by trucks. Significant savings can be realized if the experiment location allows for the delivery by railroad cars. In the following we will use a figure of \$30 M for the cost of 50 $kton$ of argon.

5.3.2 Cryogenics

Thermodynamics of a liquefied gas storage tank is quite different from that of a cryostat with active cooling system. The storage tank is, to a good approximation, a big boiling pot. The tank walls are the heat sources. Warm(er) argon rises along the walls to the top where it cools down by evaporation and sinks to a bottom in the middle part of the tank. These convection currents stabilize the temperature of the entire volume to be uniform within 0.01^o K over the most of the volume[31]. The temperature along the walls is 0.1^o K higher than the boiling temperature along the walls of the tank. The distribution of the liquid temperature throughout the tank volume is shown in Fig.5.2.

The boil-off gas constitutes $0.05\%/day$ of the total mass of the argon, or 25 ton in our specific case. The cryogenic system is necessary to re-liquefy this gas mass in order to avoid losses of the material. The liquefied argon is pumped back into the storage tank. This system ensures that the temperature of argon never falls below that of the freezing point, which is only 3° K below the boiling point.

To bracket the cost of the refrigeration unit we use a specific proposal of Cosmodyne Corp. for the LANNDD detector. The estimated cost was \$2.8 M for a unit with refrigeration capacity of 100 ton of liquid argon per day.

5.3.3 Purification

Argon purity is of the paramount importance and it is critical that the adequate purification system and procedures are in place to ensure that it is achieved.

The problem breaks out into several independent components:

- the delivered argon with purity levels at 1-2 ppm must be purified to below 1 ppb level

- tank walls as well as all the materials placed inside must be cleaned up to high vacuum standards

- all gas, especially oxygen, must be removed from the tank volume

- the tank with all its penetrations and feed-troughs must maintain its hermeticity and present no gas leaks.

- out-gassing products must be removed from the tank volume faster then they are produced

To set the scale of the problem we point out that 0.1 ppb purity level of liquid argon corresponds to 15 l of air inside the tank volume.
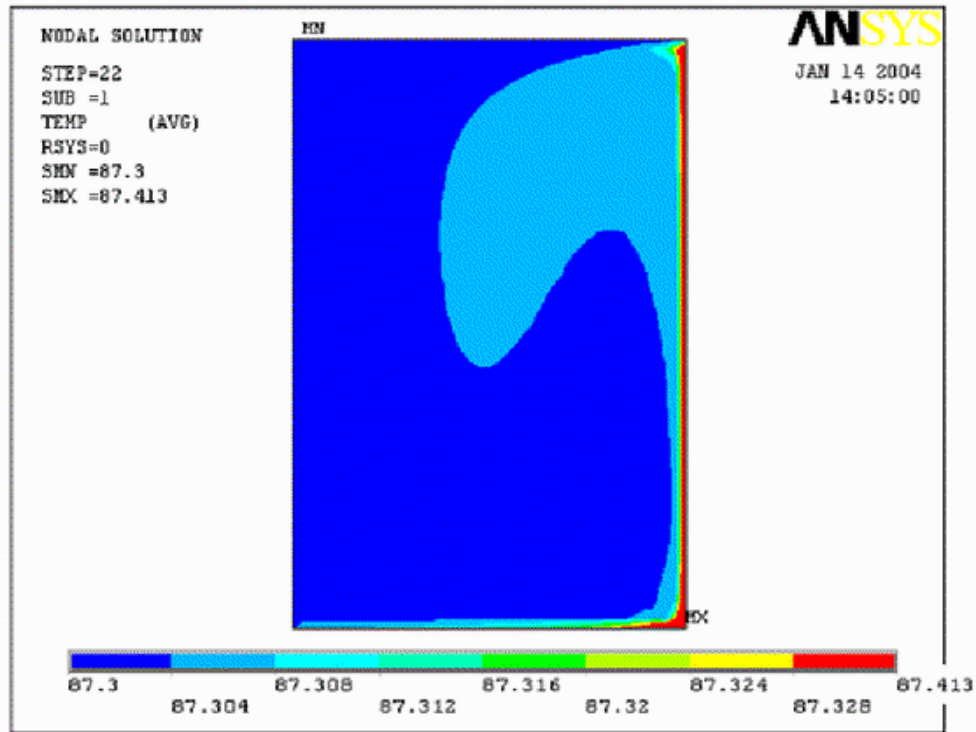
Figure 5.2: Liquid argon temperature distribution in a axisymmetric tank. One half of the tank is shown.

The inner tank surfaces, after installation of all structural elements, will be washed using diluted solution of nitric acid, rinsed with de-mineralized water and dried with dry air. The tank will become a clean room and the further operations will adhere to the clean room standards.

The tank of this construction does not permit its evacuation as a means to remove the oxygen. Instead, several volume exchanges with dry nitrogen will reduce the oxygen level to a level of about 1%. The purification process will continue with several purges of the tank volume with gaseous argon injected at the bottom of the tank. Due to higher density of the argon the gas volume will be stratified with argon gradually pushing the oxygen and nitrogen out of the tank volume. This process will reduce the oxygen level in the tank below 0.1% level, or in absolute terms, the amount of oxygen in the tank will fall below 50 kg.

It is expected that the argon will be delivered to a central location from where it will be pumped to one of the three intermediate storage tanks with

20 ton capacity through a set of purifying Oxisorb/Hydrosorb purifying filters. These tanks will be equipped with argon purity/electron lifetime detectors. If necessary the liquid argon will be recirculated at the rate of 3 $ton/hour$ through the same set of filters until the desired purity level is achieved. Batches with abnormally high impurities level, if any, will be rejected. Only argon with the purity level comparable to that in the main tank will be transferred to the main tank volume, higher at the beginning of the fill and falling gradually to 0.1 ppb towards the end.

Pure argon transferred to the main tank volume will be contaminated by the residual oxygen in the gas volume and it needs to be purified further and this will be provided by the dedicated purification systems. At the initial phase of the fill the oxygen contamination will be quite high, thus a simple distillation column will provide a cost-effective means of purification. We envisage a system of multiple heated columns with water-cooled heat exchanger with a flow capacity of 170 $m^3/hour$, or 240 $kg/hour$, which would provide a total gas volume exchange every 6.5 days at the initial phase, faster at the later stages as the tank volume is filled with liquid. This system would help to remove products of the out-gassing of the detector elements, mainly cables, which will be most abundant in the initial phase. It is likely that it will not need to be operated during the operation of the detector. A cost estimate for the construction of such a purification system (PRAXAIR) is $700K$.

To attain the desired purity level we envisage a liquid purification system using standard Hydrosorb/Oxisorb combination with a capacity of 100 $ton/hour$. This system will permit a complete liquid volume exchange in a few days in the initial phase of the fill procedure, when the total mass of the liquid is relatively low, thus permitting efficient purification. In the later phases of the the fill process the purity standard for the liquid transferred to the the tank volume will be raised accordingly on one hand and the impurities level will be reduced by the increase of the purifying effect of increased cold surfaces on the other hand.

We expect that the filling process of the tank will take about 1 calendar year. This implies handling of 200 ton of liquid argon per day. This is comparable with the capacity of liquid nitrogen handling at Fermilab.

It is expected that during the operation phase of the experiment the primary function of the purification system will be to maintain the purity level, especially by removing the out-gassing products in the gas volume of the tank. For this purpose we envisage a gas purification system with a flow capacity of 1000 $m^3/hour$.

The design and sizing of the purification system is based on the operational experience of the ICARUS T600 module. We expect that the volume-to-surface ratio should make the purification much easier in the large detector, hence probably some down-scaled system will be quite sufficient. On the other hand, given the importance of the argon purity for the functioning of the detector, we feel that substantial overcapacity is necessary to ensure reliable operation.

The cost estimate for truck stations, three twenty-ton tanks, refrigeration for the three tanks, purifiers for the twenty ton tanks, pumps to empty the
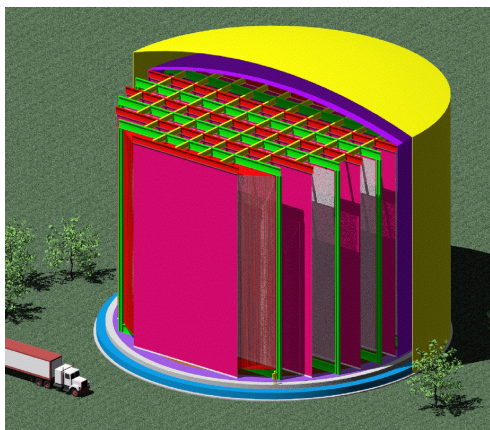
Figure 5.3: Overview of the detector inside the tank. Green planes are the wire chambers, cathode planes are in pink, field shaping frames are red (only one set is shown for clarity) . Most of the volume is free of instrumentation and it is filled with liquid argon. [Bartoszek Engineering]

tanks into the big tank, vacuum insulated transfer line from the small tanks to the large tank, pumps and gas handling for a 100 ton/hour liquid purifier and a 1000 cubic meter/hour purifier is \$6.5 M. The necessary Hydrosorb/Oxisorb filters will cost abut \$2 M.

The total cost of the handling/refrigeration and purification system is estimated to be \$12 M.

5.4 Mechanical Support Structure

The inner detector, wire chambers, cathode planes and field shaping electrodes will be supported from above by a truss formed by a set of I beams as shown in Fig.5.3.

The total load will be transferred to the floor of the building by vertical beams at the periphery of the tank.

The truss will be use also to support a flat roof of the inner tank the insulation layer of Perlite and a gas-proof membrane. The outer tank will have a domed roof as in the standard tank design. The inner membrane will be locally reinforced to provide the support for front end electronics and the access path.

Such a flat inner roof/support structure will not be able to take a significant load owing to a very large surface area of 1200 m^2. A system of relief valves and a control of the argon liquefaction process will ensure that the pressure differential of the domed volume and the gas volume of the inner tank are within the allowed range. Even for small pressure differential, however, the displacement

Element	Quantity	Total weight, lbs	Estimated cost, K$
Columns $W14 \times 730$ + gusset	12	1,234,248	30,856.20
WC1 Top Beam - $W44 \times 224$	2	59,732	1,493.30
WC2 Top Beam - $W44 \times 224$	2	53,798	1,344.95
WC3 Top Beam - $W44 \times 224$	2	39,400	985.00
Roof Truss short beams	96	119,616	2,990.40
Total			37,669.85

Table 5.1: Estimated cost of the elements of structural support of the inner detector, assuming $25.00/lb for the finished product.

of the inner roof and the supporting I-beams will be significant. It is therefore important that the inner detector design allows for vertical displacement of its support structure.

Given the size of the support structure, the requirements concerning materials purity and the cryogenic operating conditions, detailed engineering studies are necessary for a reliable cost estimate. At the moment we have evaluated the projected cost using $25.0/lb as an estimate of the construction cost, including materials and labor costs. The total cost is estimated to be $37.7 M and Table 5.1 gives more detailed breakdown.

5.5 High Voltage

An uniform electric field of 500 V/cm in the drift volume will be provided by a set of 7 cathode planes spaced 6 m apart and a collection of field shaping electrodes formed by stainless steel tube frames positioned every 5 cm between the cathode and the wire chambers as shown in Fig.5.4.

Seven independent HV power supplies with 150 kV rating will be used. HV feed-through similar to the ICARUS design will be used, the main difference being the length of the ultra-high molecular weight polyethylene insulator. The HV feedthroughs will be positioned at the periphery of the tank, nevertheless they must penetrate the outer roof, the thermal insulation layer and the gas volume in the inner tank. It is likely that the total length of the necessary insulator will be of the order of $3m$.

The cathode planes will be constructed from thin perforated stainless steel sheets and suspended from the I-beams through a set insulators. The liquid argon level control will be constructed to ensure that the cathodes are always fully submerged in the liquid.

Uniform electric field is achieved by linear gradation of the potential in the space between the cathode and the wire planes. This is achieved with a set of frames constructed from the stainless steel tubes. Four independent resistor chains degrade the potential in a linear fashion. The dimensions of the field shaping frames conform to the local tank dimensions. The frames are supported
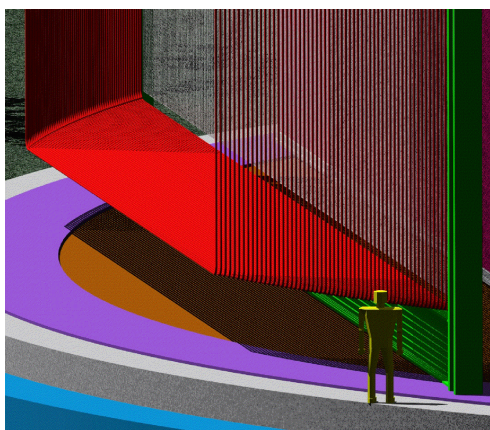
Figure 5.4: The drift volume and the field shaping cage. The green beam supports the wire chamber, the cathode plane at the left edge is removed for clarity. [Bartoszek Engineering]

from the insulated beams perpendicular to those supporting the cathodes and the wire chambers. The bottom of the frame is supported off the floor through a set of insulating stands.

The total cost of the High Voltage system is dominated by the construction cost of the cathodes and the field shaping frames. Detailed engineering studies are necessary for a reliable estimate. Using, as before, $25.00/lb as an estimate of the total construction costs we arrive with the expected cost of $5.7 M. A more detailed breakdown is shown in Table 5.2.

Element	Quantity	Total weight, lbs	Estimated cost, K$
Cathode top beam 1, $W36 \times 135$	1	18,313	457.83
Cathode top beam 2, $W36 \times 135$	2	34,912	872.80
Cathode top beam 3, $W36 \times 135$	2	29,210	730.25
Cathode top beam 4, $W36 \times 135$	2	15,764	394.10
Field shaping electrodes	708	131,579	3,289.47
Total			5,744.44

Table 5.2: Estimated cost of the elements of the HV field cage, assuming $25.00/lb for the finished product.

5.6 Wire Planes

Drifting electrons will be detected/collected with a set of wire planes positioned in the middle between the cathode planes. The drift distance is $3\ m$. Two back-to-back chambers are detecting electrons coming from opposite directions. Every chamber is composed of three wire planes: $+30^o$, -30° induction planes and a collection plane with vertical wires. The collection plane is furthest away from the cathode plane.

The wire lanes have very large dimensions: the biggest one is $30 \times 40\ m$ with the wire lengths ranging up to $36\ m$ and their construction will present a significant engineering and technical challenge. The main issues are:

- stringing and tensioning of very long wires,

- large wire capacitance which determines the electronics noise,

- large forces on the support frame,

- the survivability during the cool-down phase of the experiment

The most critical issue is quality control of the produced chamber: wire replacement is not possible on one hand and a single broken wire can short the entire drift gap thus taking a significant section of the detector out of operation.

To minimize the electronics noise it is important to keep the detector capacitance at a minimum. In ICARUS geometry, with $3\ mm$ wire spacing and $3\ mm$ spacing between plane the capacitance of the wire is $20\ pF/m$. Wire spacing determines the frequency of sampling of charged particle trajectory and the minimum track length detectable as a trajectory. For relatively simple topologies of neutrino interactions in the energy regime of the NuMI neutrino beams a $5\ mm$ wire spacing is fairly adequate. Increasing the wire spacing to $5\ mm$ increases the minimum ionizing particle signal size by 60% and it decreases the wire capacitance (and the electronics noise associated with it) by 30%[32], in comparison with the ICARUS case. It is worth mentioning that the wire capacitance varies approximately like $1/r$ and further increase of the wire spacing offers very small reduction of the capacitance.

Since there is no gain at the wire large diameter wires can be used in the detector construction. We plan to use $150\ \mu$ thick stainless steel wire. To ensure the wires' stability they will be tensioned with 10 N force, similar to that of the ICARUS T600 module, and constrained with spacers every $5\ m$. As the result the chamber frame will undergo a compressive force of about $10,000\ N/meter$, $\sim 1\ ton/m$, or $40\ tons$ for the longest chamber. This will require a supporting beam with adequate stiffness. Additional problems of wire construction, ensuring the tension uniformity and survivability of wires during the cool-down phase are addressed by the construction technique, described below.

The wires will be grouped in batches of 16 wires. The 16 individual wires will be attached with a slipknot to stainless pins and inserted into a PEEK board (side A) which will determines the wire positions. A required length of 16 wires

will be wound on an auxiliary spool with spacers inserted every 5 m. The ends of the wires will be threaded through another PEEK bar (side B) which will ensure proper wire spacing an the other end of the chamber and attached with a slipknot to a PEEK ring.

The spools will be positioned on the upper level of the supporting beams inside the detector tank and unwound dropping the PEEK board (side B) to the floor where The PEEK board will be attached to a horizontal bar determining the wire position. Below the positioning bar there will be sets of tensioning weights 1.3 kg each attached to stainless string with hooks. Every wire of the chamber will have its own weight attached to the PEEK ring at the end of the wire. This system will result in:

- a simple and practical construction technique. The required accuracy of the wire length at the construction phase will be at the level of several cm, limited by the vertical space for movement of the weights. This may be contrasted with the precision of 100 μ required for the ICARUS chambers.

- proper tension for every individual wire. This tension will be constant during all phases of construction, independent of the progressively larger deflection of the support beam as the as large portions of the wire plane are installed.

- simple procedure to test by over-stressing of every wire by putting an additional test weight on it for a short while

- no over-tension and no risk of wire breaking during the cool-down process. Since the wires have a smaller heat capacity than the supporting structure they will shrink earlier that the frames but this will only result in a change of the heights of the weights.

- the regularly spaced pins of side A allow for a simple mass terminated connection of the electronic readout cables

The procedure described above works well for the vertical plane of wires. For the stereo wires the modifications are minor: the bottom PEEK board (side B) must be displaced horizontally by 17.3 m before attachment to the positioning bar. The PEEK board will have shaped channels to guide the wires through a 30° turn before the attachment to the tensioning weight.

The chamber construction technique described above will have to be appropriately modified for the installation of stereo wires that either originate or terminate on the side support beams.

The cost of the chamber construction is likely to be dominated by the labor necessary to string approximately 300,000 wires, and this should be largely a function of number of wires only since the length-dependent component of the labor is rather small.

At present the best estimate is that it will cost about \$0.8 M to construct a single chamber (6 planes), hence the total cost of chamber construction is expected to be \$5 M.

5.7   Electronics

ICARUS collaboration has developed a complete chain of readout electronics which was demonstrated to perform adequately for a large surface detector. There are several decisions to be made in the electronics area, the primary one being the placement of the electronics inside or outside the cryostat. These decisions have repercussions for many other detector elements like chamber geometry, cables, feed-troughs etc..

Rapid progress in electronics and advances in experimental techniques driven by other large detectors (like liquid argon calorimetry of ATLAS) can influence the decision regarding readout electronics: better solutions can be had for the same cost or the old solutions can implemented with lower costs.

In this chapter we try to argue that a realistic, proven to work detector can be constructed with well understood costs, hence we accept all the technological choices adopted by the ICARUS collaboration: all electronics outside the detector cryostat. Such a detector can be built and it will function, as shown by the T600 operation. It does not require any significant R&D effort, hence it can be used as a baseline. It is very likely that better and/or cheaper detector can be constructed taking advantage of the advances in electronics and we discuss several possible improvements in Chapter 8.

The parameter of the electronics is the noise generated at the input of the first transistor. For the JFET technology and $1\ \mu sec$ shaping time, as used in the ICARUS case, this is $ENC = (500 + 2.6C) electrons$, where C is the detector capacitance in pF. The figure of merit if the experiment is S/N for the minimum ionizing track. For the detector described in the preceeding sections $S \sim 25,000$ electrons, assuming that the argon is purified to the level corresponding to the electron lifetime exceeding 10 $msec$.

The wire capacitance is 450 pF for the collection wires and up to 520 pF for the stereo wires. All the wires are read out on top. A fraction of the stereo wires terminate at the sides of the chamber and they would require much longer cables thus leading to a substantially higher noise. Three planes of readout provides an over-constrained measurement, whereas two planes are sufficient to determine the space point. We propose to to read out only stereo wires terminating at the top of the chamber, thus ensuring good signal-to-noise ratio. Such a scheme will provide a good stereo measurement over the entire area of the chamber and will provide redundant measurement over more the 60% of the area. The cable length is related to a number of penetrations for feed troughs. We envisage a chimney over 3 m to keep the cable length below 4 m, hence the cable capacitance below $180 - 200\ pF$. The heat load induced by a penetration is estimated to be 40 W hence the total heat leak of the penetrations will require an increase of the refrigeration power by abut 5%.

The total capacitance of the detector will be of the order of $650 - 720\ pF$ thus giving the expected noise figure of $2200 - 2400 electrons$ for collection and stereo wires respectively thus giving the S/N figure to be 11.4 and 10.4. While these numbers are very comfortable, they do indicate that the argon purity levels must not fall much below their design values.

Although we find the overall design of the ICARUS electronics to be of very good quality and be perfectly acceptable for a very large detector its implementation with discreet components is very expensive. It appears relatively straightforward to implement this electronics as an custom-made ASIC to reduce the price. Another, relatively straightforward improvement could be a change of the technology of the input transistor from JFET to bipolar or GaAs. It may lead to a reduction of the electronics noise by a factor of $1.5 - 2$ and boost the S/N figure accordingly.

The readout scheme of the putative detector will therefore be the following:

- a flat twisted pair cable is connecting the a set of wires to a connector on PC feed-through

- printed circuit feed through is bringing the signals to the outside of the thermally insulated volume

- short cable is transporting the cable to the FEE board with ASICs located in a VME crate

The cost of production of 300,000 channels of ASIC-based electronics is estimated to be \$1 M, including the necessary engineering. At such a level it is very likely that the cost of the entire readout system will be dominated by other costs: cables, connectors, feed-troughs, VME crates. We estimate that \$5 M should be a safe estimate of the cost of the entire readout.

5.8 Data Rates in a Surface Detector

Signals from all the wires will be digitized with frequency of 2.5 HMz. Assuming 4 bytes per digitization it sets the requirement for the data acquisition system to handle data rates of 3 $Tbytes/sec$. This is well within capabilities of a modern data acquisition systems but it requires an LHC-class DAQ.

Most of the time buckets, or 'pixels' are empty. An advanced signal processing techniques, already implemented in the ICARUS electronics (DAEDALUS chip) can perform cluster finding and baseline subtraction thus reducing the data rate into the DAQ system by a large factor. The resulting data volume is dominated by the signals induced by cosmic muons. The rate of cosmic muons crossing entering the detector is about 200 kHz. Most of them range out in the upper part of the detector. Their angular distribution leads to a relatively few wires being hit. This is, in fact, a significant factor to be taken into account in the specification of the front end electronics, as it leads to a very large dynamic range of the input signals. As a safe upper limit we assume that the average number of wires hit by a cosmic muon is less than 2000. The expected data rates is therefore less than 1.6 $Gbyte/sec$. Muon induced electromagnetic cascades can produce higher occupancy but they are infrequent enough not to contribute to the average data rates.

In an accelerator experiment with external beam timing (providing a time reference, T_0) a beam duty factor reduces the data volume by a factor of 10^3.

Detector subsystem	estimated cost in \$M
Cryogenic tank	11.0
Liquid Argon(delivered)	30.0
Refrigeration and Purification	12.0
Structural Supports	37.7
High Voltage and Field Shaping	5.7
Inner Detector	5.0
Electronics	5.0
Data Acquisition and Storage	5.0
TOTAL	111.4

Table 5.3: Estimated cost of the 50 kton Liquid Argon Off-axis Detector.

We envisage the detector to be a tool for a wider range of physics topics than the appearance experiment, hence we a more powerful data acquisition system is appropriate. The eventual cost is likely to be dominated by the cost of data storage and distribution system. Major savings can be realized with intelligent data compression techniques or with removal all of the recognized cosmic muons from the data sets.

We estimate that the cost of the data acquisition system and the necessary data storage systems will be of the order of \$10 M.

5.9   Total Detector Cost

The detailed cost estimate does require a more detailed engineering studies. The detector described here is of un-precedented scale on one hand, but it is relatively simple on the other hand. A significant fraction of the total cost are the industry-provided items (tank, argon, refrigeration systems, purification systems) whose costs are relatively well known as the scale of our application is quite typical in the industrial systems.

This cost may be contrasted with the construction cost of 1.2 $kton$ ICARUS module, which is of the order of \$25 M. The difference is huge and must be understood and explained. It is largely due to the difference related to the space and safety requirements of the Gran Sasso experiment and to the advances of the electronics industry as well as to the advantages of the large detectors in terms of the volume to surface ratio. As an example, a total number of wires for 40 times bigger Off-axis detector is only five times larger that that in the T1200. It is instructive to point out that the cost of the liquid argon is the dominant cost of the large detector is a minor cost element of the T1200.

Here the main differences between the Off-axis detector and the T1200:

- large industrial cryogenic tank vs thin-walled, custom cryostat with the active thermal shield. The cryostat and associated cryogenics costs cover about 40% of the T1200 module.

- discreet components electronics (the second largest cost element) is a very expensive solution. Advances in the electronics area make custom ASIC much more economical solution. The scale of the necessary readout electronics is very similar to the electronics of the upgraded silicon detectors of D0 and CDF, hence the cost estimate is probably very realistic.

- large volume of the detector allows for simple mechanical solutions for the inner detector system, thus reducing the construction costs considerably.

On the other hand it appears surprising that the cost of the high-performance imaging detector appears to be comparable or even lower that that of an inferior sampling calorimeter detector. This can be understood as a being do to the following factors:

- a detector hall for a very large detector has a significant cost associated with it $25−30\,M$. This is substantially higher that the cost of the storage tank.

- the cost of the liquid argon is comparable to a OSB absorber and within 50% of the cost of of the particle board.

- a number of detector channels is comparable or actually smaller in case of the liquid argon owing to a long drift distances. These detector channels, wires, are relatively simple yet they provide far more detailed information than the traditional detector.

5.10 Detector Site

To first order, the optimal site location for neutrino oscillation detector is that which maximizes $\sin^2 1.27\frac{\Delta m^2 L}{E}$. For the present best value of the atmospheric Δm^2, the oscillatory term is maximal for an L/E of 450 to 500 km/GeV. Matter effects favor a longer baseline (L) while flux considerations (number of events) favor a shorter baseline. The NuMI off-axis beam at an off-axis angle of ~13.7 mrad exhibits the best combination of maximum flux and sharp peaking in energy. This corresponds to a mean beam energy of around 2 GeV giving an ideal baseline of 850 to 900 km.

Further desirable characteristics for the experiment site are:

- access by rail to minimize transportation costs,

- proximity of a highway that is maintained year-round,

- stable local geology,

- location not too close to a populated area,

- availability of a wide lateral area (i.e., spanning a range in off-axis angle) so that the choice of exact location can be made to optimize the physics potential.

A location which satisfies all these criteria is located near the western boundary of the Canadian province of Ontario. The nearest town, Fort Frances, is about 60 km west and borders the American city of International Falls. The small village of Mine Centre is about 15 km east of the site. The central NuMI beam axis is about 8.7 km above the surface at this point and the site for the 13.7 mrad off-axis beam is then about 8.6 km east of the central beamline. Just as an illustration of the siting flexibility associated with this location, we notice that there is also a suitable site at the 12 mrad off-axis. Sites to the west of the central beamline would be located in a First Nations reserve and so were not considered further.

All sites to the east of central beamline are on crown (public) land and so land use should not be an issue. It is possible to locate the detector quite close to the railroad. Depending on how close it is feasible to get, rail spur costs can be as low as several hundred thousand dollars. All sites are a few km north of Trans-Canada Highway 11 which is a main highway maintained year-round.

The major port city of Thunder Bay is around 360 km east allowing for the possibility of transporting the liquid argon by ship most of the way and then transferring it to a train for final transport to the site. The basic underlying geology of the region is granite, hence the area is very stable geologically.

Chapter 6

Small Liquid Argon Detectors

Experience gained with successful construction and operation of the T600 module of ICARUS allows for a relatively straightforward design of smaller detectors suitable for Fermilab's neutrino beams. They can be placed in the near MINOS hall or in a dedicated new experimental hall in the MiniBOONE beam. As an example we describe a possible design of a 40 ton detector, T40[51], but with a relatively straightforward extrapolation such a design can be scaled to detectors in the range $20 - 100\ ton$.

6.1   T40 Detector

The detector is constructed as a cylinder filled with liquid argon (see Fig.6.1). A vertical wire chamber (item 1) is aligned along the cylinder axis and splits the volume into two drift regions (left and right).

A horizontal and uniform electric field is generated in each region by a cathode (4) and a system of field shaping electrodes(3).

The chamber is built of two sets of wire planes. An additional central grounded wire plane screens the left and the right sets one from the other.

Signals from wires are brought to the front-end electronics, outside the cryostat, through twisted pair cables and low voltage feedthrough flanges (5). Two high voltage feedthroughs (6) are used to bias the cathodes and the field shaping electrodes.

The vacuum insulated and liquid nitrogen cooled cryostat is built of an inner vessel and an outer vessel, with vacuum in between. The inner vessel is surrounded by a dimpled surface jacket welded to it and refillable with LN2. Three square frames are part of the outer vessel. They are used as bases for it and as supporting frames for the inner vessel. Wrapping the inner vessel and the LN2 jacket by super-insulation layers and suspending them to the outer vessel frame by three steel belts (11) minimize the heat input.
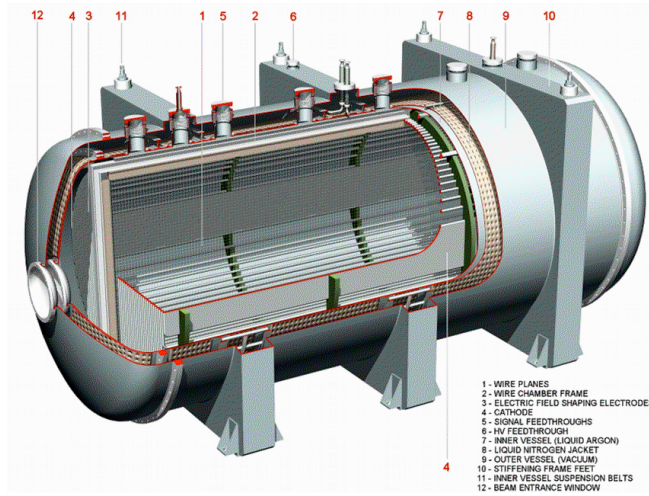
```
1 - WIRE PLANES
2 - WIRE CHAMBER FRAME
3 - ELECTRIC FIELD SHAPING ELECTRODES
4 - CATHODE
5 - SIGNAL FEEDTHROUGHS
6 - HV FEEDTHROUGH
7 - INNER VESSEL (LIQUID ARGON)
8 - LIQUID NITROGEN JACKET
9 - OUTER VESSEL (VACUUM)
10 - STIFFENING FRAME FEET
11 - INNER VESSEL SUSPENSION BELTS
12 - BEAM ENTRANCE WINDOW
```

Figure 6.1: T40 Detector: cutaway view.

The main parameters of the T40 detector are reported in Table6.1. The low nitrogen consumption allows operating the detector with a reduced size, refillable nitrogen storage dewar.

A relatively small size of the described detector with respect to the T600 module of ICARUS allows for significant simplifications of the construction and cryogenics, vacuum insulation being the prime example.

Construction cost of such a detector can be reliably estimated from the experience of the ICARUS module construction[52].

These cost estimates, Table 6.2 are valid for a construction in a surface hall. They are probably accurately estimate of a construction in a possible new hall in the MiniBOONE beam. A construction of a possible T40 class detector in a near MINOS hall (Fig.6.2 would be complicated by the size of the NuMI access shaft. In this case the cryostat needs to be constructed in place, nearly doubling the estimated cost of the cryostat.

6.2   Near Liquid Argon Detector in an Underground Hall

An operation of a liquid argon detector in an underground hall requires careful analysis of the installation and operation and the safety aspects.

To put the upper limit on the associated costs we have considered the case of the operation in the near MINOS hall, some $100 \, m$ underground[53]. Installation and operation in a dedicated hall in the MiniBOONE beam would be

Active liquid argon sizes	Φ = 2.4 m, L=6.0 m
Active liquid argon mass	38.5 Ton
Number of drift regions	2
Max drift lengths	2 1.2 m
Maximum required high voltage	60 kV
Number of cathode planes	2
Number of wire chambers	1
Number of readout wire planes	4
Orientation of readout wires	0, 90
Number of readout wires	5632
Heat Input a) Radiation (with wr = 1 watt/m2) b) Conduction (cables + mech. supports) Total	 72 W 240 W 312 W
Equivalent liquid nitrogen consumption	0.2 m^3/d
Dipole magnet (warm, B = 0.6 T) Copper weight Power @ 35 kA Iron yoke	 60.2 Ton 2.5 MW 900 Ton

Table 6.1: T40 - Parameters

considerably easier and cheaper, but such an experimental hall would have to be constructed.

Cooling would be provided by liquid nitrogen piped through vacuum insulated lines from the surface and the gaseous nitrogen returned to the surface. There would be no liquid argon storage on the surface: the tank would be filled directly from the supply trucks. If necessary the argon would pumped to the surface and vented. A detailed study would be required to evaluate and mitigate the oxygen deficiency hazard, but an it is not expected to be a major issue.

Underground operation will lead to significant costs of the additional equipment, installation and testing and analysis of the safety requirements.

These costs are estimated to be $250 K for materials and services, 70 man-weeks of engineering effort and 178 man-weeks of technician effort.

6.3   Magnetic Field?

The possibility of operating liquid argon TPC's in magnetic field is, by far, the most interesting implementation of this kind of detector. This feature allows easy muon sign discrimination and momentum evaluation. At beam momenta lower than 5 GeV/c, with a magnetic field intensity of 0.6-1.0 T, calculations indicate that the sign discrimination for e that initiated an electromagnetic shower becomes possible too. The main parameters for a possible configuration

| Liquid argon	$60m^3$	$30K
Cryostat	Inner vessel	
	LN2 jacket	
	Outer vessel	
	Beam entrance windows	
	Chimneys for signals, HV,	
	IN/OUT Ar, IN/OUT LN2,	
	inner vessel suspension	$500K
Inner detector	Wire chamber (frame, wires)	
	Field shaping electrodes	$70K
Electronics (5632ch.) and DAQ	Signal cables	
	feedthroughs	
	Analog and Digital crates	
	Calibration pulser	
	Wire bias HV power supplies	
	Data acquisition computer	$350K
Vacuum & cryogenics	Vacuum pumps and gauges	
	LN2 and LAr storage dewars	
	LAr purification system and purity monitor	
	Transfer lines, valves	
	Level and temperature monitors	$75K
High voltage system	Power supply, feedthrough, monitor	$25K
Other systems	External trigger counters and electronics	
	UPS and O2 monitors	$150K
Total		$1200K

Table 6.2: T40 - cost estimate
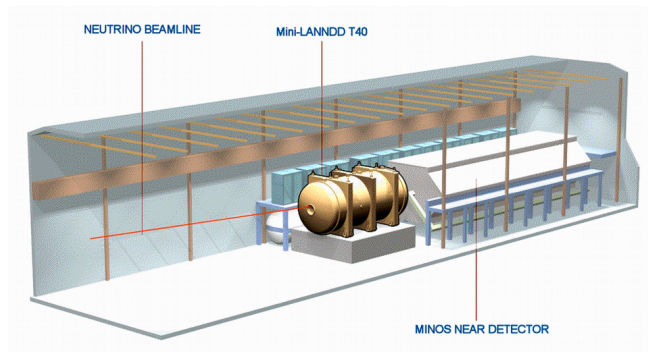
Figure 6.2: T40 detector located in the near MINOS hall. The near MINOS detector serves as a muon catcher. The detector is raised to the nominal height of the incoming neutrino beam.

with a dipole magnet are indicated at the end of Table6.1.

Such a configuration would enhance the physics potential of T40 detector for the studies of low energy neutrino interaction and it would be of major interest for the future experiment at neutrino factories. Given the cost and associated complications one would probably consider addition of a magnet as a second phase of the possible experiment.

Chapter 7

Double Beta Decay Experiment with a Liquid Argon Imaging Detector

7.1 Double beta decays and neutrinos

Interest of neutrino-less double beta decays ($0\nu\beta\beta$) has recently been sharpened since they may have discovery potential for the Majorana neutrino masses and other fundamental properties of neutrinos [56].

Fundamental neutrino properties to be studied by $0\nu\beta\beta$) are the Majorana nature of neutrinos, the type of mass spectrum, the absolute neutrino mass scale and possibly the CP violation. Actually, $0\nu\beta\beta$ experiments is the only practical method for studying all these important properties of neutrinos in the foreseeable future.

The data from Super-K, SNO and KamLAND, together with their theoretical analyses, clearly imply that next-generation experiments with the mass sensitivities of the atmospheric ν-mass scale (50 meV) should discover non-zero effective Majorana electron neutrino mass if the massive neutrinos are Majorana particles and the neutrino mass spectrum is of the quasi-degenerate type or with inverted hierarchy. In fact, many theories of the fundamental particle interactions predict that the massive neutrinos are Majorana in nature. Experiments with even higher sensitivies of the solar ν-mass scale(a few meV) are of potential interest for further studies in case of normal hierarchy and possibly of the CP violation.

Since $0\nu\beta\beta$ events are extremely rare low-energy processes, the experiments require large amount($\sim$ ton) of $\beta\beta$ isotopes, large-scale low-background detectors and very stringent selection of the signal from background events. The $0\nu\beta\beta$ rate depends on the nuclear matrix element as well. Accordingly it is indispensable for identifying the $0\nu\beta\beta$ event to perform at least two or three

independent experiments utilizing different isotopes and methods. Here the different methods should include the calorimetric method with active source detectors and the spectroscopic β-tracking method with external sources.

7.2   MOON

The nucleus ^{100}Mo has large responses for both the $\beta\beta$ decay and low-energy solar and supernova ν's [57]. Thus Majorana neutrino masses and the charged-current interaction of solar and supernova ν's can be studied effectively using ^{100}Mo.

The MOON (Molybdenum Observatory Of Neutrinos) project [58] is a hybrid $\beta\beta$ and solar ν experiment with planned sensitivity to Majorana mass of the order of $< m_\nu > \sim 0.03$ eV as well as capability for spectroscopy of pp and ^{7}Be solar ν's.

The two β rays from ^{100}Mo are measured in prompt coincidence for the $0\nu\beta\beta$ studies. The large Q value of $Q_{\beta\beta}$=3.034 MeV gives a large phase-space factor $G^{0\nu}$ to enhance the $0\nu\beta\beta$ rate, and the energy and angular correlations for the two β-rays are used to identify the ν-mass term for the $0\nu\beta\beta$.

Low energy solar-ν captures are measured in delayed coincidence with the subsequent β decay of the 16-second daughter ^{100}Tc. The low threshold energy of 0.168 MeV for the solar-ν and the large capture rates allow real-time studies of pp and ^{7}Be ν's. With a low threshold energy and large GT and spin-dipole strengths, ^{100}Mo is also sensitive to electron ν's from supernovae.

The measurement of two β-rays (charged particles) enables one to localize in space and in time the decay-vertex points for both the $0\nu\beta\beta$ and solar-ν studies. The localization is crucial for selecting $0\nu\beta\beta$ and solar-ν signals and for reducing correlated and accidental backgrounds.

MOON is required to have a large amount ($\sim$ one ton) of ^{100}Mo isotope (whether natural or enriched) and good energy and position resolutions. Research and development of possible detector options are in progress. They include supermodules of plastic fiber scintillators, liquid scintillators, cryogenic bolometers and others. The Mo source and scintillator are to be purified to the level of1 ppt [59].

7.3   Double Beta Decay Experiment with Liquid Ar

Liquid Ar detectors have several merits for studying $0\nu\beta\beta$. We briefly discuss the energy resolution, the position resolution, and the background rate, which are crucial for high sensitive studies of double beta decays.

The energy resolution of the liquid Ar detector itself is very good as shown in Fig.7.1 [60]. A significant contribution to the energy resolution is due to the energy loss in the Mo foil. Noting that the two beta rays from the $0\nu\beta\beta$ event are emitted opposite with each other, we measure such 2 β rays above 0.5
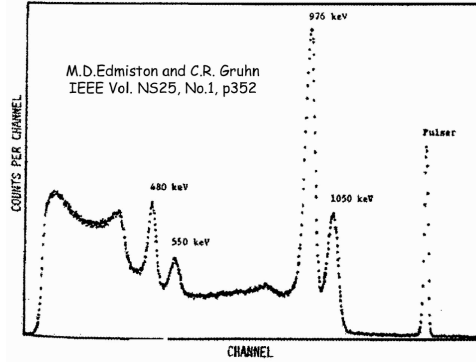
Figure 7.1: The pulse height spectrum of ^{137}Cs measured with liquid argon ionization chamber. The energy resolution, limited by electronics, is $\Delta E/E = 0.015$ at $E = 976\ keV$

MeV. Then the energy spread of the sum of the $\beta\beta$ rays is given as FWHM $= \delta E(\sqrt{2}-1)$, where δE is the foil thickness. Using the Mo foil with 30 mg / cm^2, one gets FWHM $= 20$ keV, which is only 0.7 %. Thus it is possible to carry out a high resolution (FWHM $\leq 1\%$ experiment even with the Mo foil.

The major BG of the liquid Ar detector comes from the impurities of the radioactive ^{42}Ar. It decays with $T_{1/2} = 33$ y and $Q = 0.6$ MeV to ^{42}K, which decays successively to ^{42}Ca with T$_{1/2} = 12.4$ hr and Q $= 3.52$ MeV The β decay with 81% branch to the ground state can partly invade into the $0\nu\beta\beta$window.

The BG rate per year per 1 ton ^{100}Mo is evaluated as

$$Y(^{42}K) = aM\epsilon\ 2.6 10^{26} \tag{7.1}$$

where a is the ^{42}Ar impurity ratio , ϵ is the efficiency and M is the mass ratio of Ar to Mo. M can be $M \sim 30$ to stop most of β rays below 2 MeV. The efficiency is estimated to be $\epsilon \sim 2 10^{-5}$. It is noted here that most of the β rays from ^{42}K with the half-life of 12.4 hr can be rejected by looking at the preceding β decay from ^{42}Ar by using adequate segmentation. Thus the GBG rate per year ton is $Y(^{42}K) = a\ 1.5\ 10^{23}$.

It should be noted that most RI impurities(natural and cosmogenic) do not come into the $0\nu\beta\beta$ window because of the quite high $Q_{\beta\beta}$. The ^{214}Bi β can be rejected by measuring the post α decay after 100-200 micro sec.

The ^{42}Ar impurity is reported to be $a \leq 10^{-21}$. Then one gets $Y(^{42}K) \leq 1.5\ 10^2$. This corresponds to the neutrino mass sensitivity of the order of 50 meV for 5 year measurement with 1 to ^{100}Mo. Thus we need R&D to reduce further the impurity of ^{42}Ar to the level of $\leq 10^{-22}$ in order to achieve the mass sensitivity of the order of 30 meV.

The $2\nu\beta\beta$ contribution to the $0\nu\beta\beta$ window can be negligible in the present case of the energy resolution of FWHM $= 1 \sim 2\%$.

The position resolution is required to reduce the $2\nu\beta\beta$ BG at the solar neutrino window. The inverse β ray from the ^{7}Be solar neutrino is measured in the delayed coincidence with the successive β decay of ^{100}Tc. Using the time window of 30 sec, The accidental rate at the ^{7}Be window is

$$Y(\beta\beta) = \epsilon' \ 2.6 \ 10^7 \ K^{-1} \qquad (7.2)$$

where ϵ' is the efficiency and K^{-1} is the position resolution in unit of ton. Assuming a modest efficiency of $\epsilon' \sim 5\%$, the position resolution of around $K^{-1} = 10^{-7}$ is required. This corresponds to 0.1 g of ^{100}Mo, i.e. 2 cm × 2 cm for the foil with 30 mg/cm^2. This is well within the capabilities of the liquid argon detector.

The liquid argon TPC detects two individual β- tracks emitted opposite to each other to identify the $0\nu\beta\beta$. This is unique among other high sensitive calorimetric experiments.

7.4 Liquid Argon Detector

The detector takes advantage of the Mo foils using them as cathode planes. The drift distance required to contain fully the electron tracks is 2 cm, hence the argon purity requirements are relaxed by about two orders of magnitude compared with the ICARUS module.

The fundamental detector cell consists of a cathode plane and two wire chambers (two wire planes, X and Y, each) on either side of the cathode for a total thickness of 5.5 cm. To ensure required position resolution the wire pitch is 1 cm. As every cell provides a complete measurement of the $0\nu\beta\beta$ decay the detector can be constructed in a modular fashion, if so desired.

A detector for 1 $kton$ of enriched molybdenum appears relatively straightforward (especially in comparison with the enrichment itself. It would be somewhat smaller than ICARUS test module and it would contain about $400ton$ of liquid argon. The main parameters of a possible monolithic detector are summarized in Table7.1.

This detector is very similar, conceptually, to the one operated in Gran Sasso laboratory [61]. Such a detector can be constructed using the existing technology, the prime challenge being the molybdenum enrichment. The most critical detector performance parameter is the energy resolution which is, turn, limited by electronics noise, which is related to the detector capacitance. The wire capacitance is minimized by relatively large wire spacing and little improvement can be expected here.

Possible development of a new amplifier using other than JFET technology is one possible avenue. The biggest improvement can be attained by development of a cold version of the readout electronics which is mounted directly on the chambers inside the cryostat. Such a solution would eliminate the cables, which are the dominant contribution to the source capacitance. Low operating temperature would reduce further the electronics noise.

Cryostat cross section (inner)	$4.5 \times 4.5 \ m^2$
Cryostat length	$14 \ m$
Mass of liquid argon	$397t$
Cathode plane (^{100}Mo) thickness	$25 \ \mu$
Cathode plane size	$4 \times 4 \ m^2$
Number of cathode planes	250
Wire chamber dimensions	$4 \times 4 \ m^2$
Number of wires planes/chamber	2(X and Y)
Wire pitch	$1cm$
Total number of chambers	500
Total number of wires	400,000
Total number of electronics channels	400,000

Table 7.1: Parameters of 1 $kton$ ^{100}Mo double beta decay detector

Chapter 8

Proposed R&D Program

In the preceeding chapters we have argued that a liquid argon technology with the very fine spatial granularity, good energy resolution, good particle detection and identification and imaging capabilities opens a qualitatively new phase in neutrino experiments.

This is a mature technology. Detectors can be constructed based on the knowledge we have in hand and they can be surprisingly inexpensive. It does sound too good to be true. The primary goal of the proposed R&D program is to establish a credibility of this proposition. Once this credibility of the technical claims is established we envisage a number of possible improvements to the existing technology, thus making the detectors cheaper for a given performance, better for a given cost or more reliable.

A successful completion if the R&D activities described below is necessary to make credible and defendable proposals of the future experiments. Total required resources are:

- 12 months of engineering support

- 200 K for materials and services

- space and technical support for the construction of the small detector prototype

8.1   Establish Credibility of the Experimental Proposals

In this letter we have made two assertions:

- high-performance liquid argon "Near Detector" of 40 $kton$ class can be constructed by simplifying and scaling down the ICARUS T600 module. Such a detector can be constructed in a relatively short time scale and it would offer a very attractive neutrino physics program

- a very large surface detector can be constructed using existing liquid argon technology combined with the industrial techniques for cryogenic liquid storage, refrigeration and purification

Given the potential payoff in terms of the physics potential we think it is very important to demonstrate credibility of these claims. This is the primary goal of the proposed R&D program.

8.1.1 'T40' Detector

The detector is a simplified and scaled down version of the ICARUS module. The main differences are:

- small, simplified vacuum insulated cryostat

- cylindrical rather than rectangular drift volume (this should have little bearing on the performance and construction though).

All of the technical aspects of such a detector are already demonstrated by the ICARUS collaboration. Scarcity of the first technical expertise in the US is the chief obstacle in making a detector proposal. We propose to address this by a construction, in collaboration with the ICARUS colleagues, of a small TPC module as a means of the 'technology transfer'.

A successful operation of such a chamber, expected to be in the 100 l of liquid argon, 80 cm drift distance range, will provide an important proof of the relative maturity of the technology itself. Such a chamber is under construction using bits and pieces borrowed from ICARUS and from various Fermilab shops. To maximize the chance of a success this project requires some $100K$ to procure some cryogenic elements, purification filters etc.. With the collaboration of the ICARUS colleagues we hope to bring this prototype into operation no later than the spring of 2005.

A proposal for an experiment using small LaR TPC requires a detailed safety analysis related to possible hazards of operation in confined, perhaps underground locations and the related cost implications. For the case of an experiment located in the near MINOS hall additional costs of an undergrond construction must be analyzed. An initial analysis shows that all the problems can be addressed with no serious cost implications, but we expect that some 3 months of engineering work is necessary to have full confidence in the conclusions.

8.1.2 50 kton Detector

This is an extrapolation of the ICARUS module based of the established facts:

- liquid argon can be purified to levels enabling drift distances up to 3 m

- front-end electronics can be build to ensure good signal-to-noise ratio for detector capacitances up to 400 pF

The primary challenge in scaling up to much larger detector volume is to design a cost-effective detector while maintaining the detector performance. The latter reduces mostly to ensuring sufficient liquid circulation capacity through a set of commercial filters.

Cost effective solution for the large detector design is accomplished by replacing modular custom-made cryostats of ICARUS with an industrial grade liquified gas storage tank. This replacement provides the most of the cost savings, but it leads to a natural question if such a tank will permit the required purity level of liquid argon to be achieved. It is a very relevant question as the large tank solution requires that evacuation as an initial stage of cleaning must be replaced by several purges with nitrogen and argon.

The question of the ultimate argon can only be answered in situ with the ultimate detector, but a high level of confidence can be achieved by detailed engineering studies of the material purities and the purification process. To this end we plan to use the small test chamber mentioned above to investigate the relevance of various cleaning procedures as well as the influence of materials likely to be used in the final detector on the argon purity level. It is expected that the studies of the purification process will involve industry producing purifying filters. One of the suggested tests may involve purification of the liquid argon in one of the commercial nitrogen storage tanks available at the Fermilab site. We expect that the studies of the purification process and the achievable purity levels will require 3 months of engineering and $100\,K$.

Apparent simplicity of the ultimate detector suggests that the cost estimates may be fairly realistic. The devil is in details, though, and it may be that significant costs may be hidden in the details ignored so far. We estimate that 6 months of the detailed engineering effort is necessary to produce very reliable material and construction cost estimate.

Very significant cost savings, with respect to the ICARUS module, can be realized by implementation of the front end electronics in a customized ASIC. We consider this step to be well understood and not requiring a proof of feasibility. On the other hand, various further improvements in the electronics are desirable for the real experiment and they will be described later.

8.1.3 Double Beta Decay Detector

Feasibility of the liquid argon-based double beta decay experiments depends on the background levels attainable with sheet geometry on one hand and induced by Ar^{42} on the other hand. These background calculations will be carried out by Osaka and University of Washington groups.

Achievable spatial and energy resolution will be limited by the electronics noise of the detector. Optimization of the wire readout system, for example multiple induction planes to reduce the electronics noise, will be carried out with the prototype mentioned earlier.

A significant improvement can be achieved by further improvements of the low noise, high gain preamplifiers.

8.2 Future/Further R&D Efforts

Having all the results of the ICARUS efforts and profiting from a close collaboration with this group we estimate that this phase of the R&D can be carried out within one calendar year and we expect it will lead to proposals of specific physics experiments.

Being confident that these experiments will be judged important enough to become a part of the scientific program of the Laboratory we envisage further program of R&D aimed at the further improvements of the detector technology and data analysis techniques.

These studies will include:

- studies of other technologies (bipolar or GaAs) for the front end electronics to reduce the input noise and to improve signal-to-noise ratio.

- studies of a possible solution for cold electronics (i.e. electronics inside the cryostat) to reduce further the electronics noise by elimination of the cable capacitance and to reduce or eliminate problems related to cables (out-gassing, feedthroughs, etc).

- optimization or simplification of the front end electronics using modern industrial solutions (for example modern FADC for every channel instead of the multiplexing, FPGA arrays for the cluster finding, etc..)

- investigation of data analysis and event reconstruction techniques for four dimensional (including floating T0) data

- investigation of data compression, data organization and data storage technologies for the massive amount of data expected from the free-running surface detector

Bibliography

[1] S. Wojcicki, private information

[2] W. Hofman, U. Klein, M. Shultz, J. Spengler and D. Wegener, Nucl. Instrum. Meth. A **135**, 151 (1976).

[3] H.H. Chen, P.E. Condon and B.C. Barish, Fermilab Proposal P-496, May 1976

[4] H.H. Chen, J.F. Lathrop and J. Learned, "Further Observation of Ionization Detectors Drifting in Liquid Argon", IEEE Trans. Nucl. Sci. **NS-25** (1978) 358

[5] B. Kephart, private information P. Doe, private information

[6] E. Gatti *et al.*, "Consideration for the Design of a Time Projection Liquid Argon Ionization Chamber", IEEE Trans. Nucl. Sci. Vol. **NS-26** (1978) 2910

[7] C. Rubbia, "The Liquid-argon time projection chamber: a new concept for Neutrino Detector", CERN-EP/77-08 (1977)

[8] O. Bunemann,T.E. Cranshaw and J.A. Harvey, Can. J. Res **27** (1949) 191.

[9] E. Aprile, K.L. Giboni and C. Rubbia, "A study of ionization electrons drifting large distances in liquid and solid argon", Nucl. Instrum. Meth. A **241** (1985) 62

[10] E. Buckley *et al.*, "A study of ionization electrons drifting large distances in liquid argon", Nucl. Instrum. Meth. A **275** (1989) 364

[11] S. Bonetti *et al.*, "A study of the Electron Image due to ionizing events in a two-dimensional liquid argon TPC with a 24 cm drift gap", Nucl. Instrum. Meth. A **286** (1990) 135

[12] P. Benetti *et al.*, "The ICARUS R&D program and results", Nucl. Instrum. Meth. A **327** (1993) 173

[13] P. Benetti *et al.*, "A three-ton liquid argon time projection chamber', Nucl. Instrum. Meth. A **332** (1993) 395

[14] P. Cennini *et al.*, "Performance of a three-ton liquid argon time projection chamber", Nucl. Instrum. Meth. A **345** (1994) 230

[15] F. Arneodo *et al.*, "First Observation Of 140-cm Drift Ionizing Tracks In The ICARUS Liquid-Argon TPC", Nucl. Instrum. Meth. A **449** (2000) 36

[16] F. Arneodo *et al.*, "Performance Of The 10-M**3 Icarus Liquid Argon Prototype," Nucl. Instrum. Meth. A **498**, 292 (2003).

[17] P. Cennini *et al.*, "Detection Of Scintillation Light In Coincidence With Ionizing Tracks In A Liquid Argon Time Projection Chamber", Nucl. Instrum. Meth. A **432** (1999) 240

[18] M. Antonello *et al.*, "Detection of Cerenkov light emission in liquid Argon", Nucl. Instrum. Meth. A **516** (2004) 348

[19] A. Bettini *et al.*, "A Study of The Factors Affecting The Electron Life Time in Ultra-Pure Liquid Argon", Nucl. Instrum. Meth. A **305** (1991) 177

[20] S. Amoruso *et al.*, "Study of electron recombination in liquid Argon with the ICARUS TPC" Nucl. Instrum. Meth. A **523**, 275 (2004).

[21] F. Arneodo *et al.*, "Determination Of Through-Going Tracks' Direction By Means Of Delta-Rays In The ICARUS Liquid Argon Time Projection Chamber", Nucl. Instrum. Meth. A **449** (2000) 42

[22] F. Arneodo *et al.*, "Performance Evaluation of a Hit Finding Algorithm for the ICARUS Detector", Nucl. Instrum. Meth. A **412** (1998) 440

[23] P. Cennini *et al.*, "A neural network approach for the TPC signal processing", Nucl. Instrum. Meth. A **356** (1995) 507

[24] Hydrosorb and Oxisorb, Messers-Griesheim GmBH, Krefeld, Germany

[25] P. Cennini *et al.*, "Argon purification in the liquid phase", Nucl. Instrum. Meth. A **333** (1993) 567

[26] S. Amoruso *et al.*, "Analysis Of The Liquid Argon Purity In The Icarus T600 TPC," Nucl. Instrum. Meth. A **516**, 68 (2004).

[27] A. Bettini *et al.*, "The ICARUS liquid argon TPC: a complete imaging device for particle physics", Nucl. Instrum. Meth. A **315** (1992) 223

[28] S. Amerio *et al.*, "Design, construction and tests of the ICARUS T600 detector" Accepted for publications by Nucl. Instrum. Meth. A

[29] S. Amoruso *et al.* [ICARUS Collaboration], "Measurement of the mu decay spectrum with the ICARUS liquid argon TPC," Eur. Phys. J. C **33**, 233 (2004) [arXiv:hep-ex/0311040].

[30] F. Arneodo *et al.*, "Observation Of Long Ionizing Tracks With The Icarus T600 First Half-Module," Nucl. Instrum. Meth. A **508** (2003) 287 [Erratum-ibid. A **516** (2004) 610].

[31] Zhijing Tang, "Thermal Analysis of Liquid Argon Tank", engineering note

[32] Zhijing Tang, "Some Problems about the Argon Tank", engineering note

[33] F. Sergiampietri, Proc. IV Int. Conf. on Calorimetry in High Energy Physics, La Biodola, 1993, p357 S.P. Denisov, Proc. VI Int. Conf. on Calorimetry in High Energy Physics, Frascati, 1996, p125.

[34] F. Sergiampietri, "On the Possibility to Extrapolate Liquid Argon Technology to a Supermassive Detector for a Future Neutrino Factory", presented at NuFACT'01, Tsukuba, Japan, May 2001

[35] D.B. Cline, F. Sergiampietri, J.G. Learned and K.T. McDonald, "LANNDD, A Massive Liquid Argon Detector for Proton Decay, Supernova and Solar Neutrino Studies, and a Neutrino Factory Detector", presented at NuFACT'01, Tsukuba, Japan, May 2001, http://xxx.lanl.gov/abs/astro-ph/0105442

[36] G. Mulholland, "A LANDD Investigation", report, private information

[37] http://www.chicago-bridge.com

[38] D. Rahm, BNL, private information

[39] H. Minakata and H. Nunokawa, JHEP **0110** (2001) 001 [hep-ph/0108085]

[40] D. Beavis *et al*, Proposal of BNL AGS E-889 (1995)

[41] A. Para, M. Szleper, Neutrino Oscillation Experiments using Off-axis NuMI Beam, hep-ex/0110032

[42] D. Ayres *et al*, Letter of Intent to build an Off-axis Detector to study $\nu_\mu \rightarrow \nu_e$ oscillations with the NuMI Neutrino Beam

[43] Olga Mena, Fermilab, private information.

[44] Olga Mena, Fermilab, private information.

[45] K. Scholberg, "Supernova neutrino detection," Nucl. Phys. Proc. Suppl. **91**, 331 (2000) [arXiv:hep-ex/0008044].

[46] A. Bueno, I. Gil-Botella and A. Rubbia, "Supernova neutrino detection in a liquid argon TPC," arXiv:hep-ph/0307222.

[47] I. Gil-Botella and A. Rubbia, "Oscillation effects on supernova neutrino rates and spectra and detection of the shock breakout in a liquid argon TPC," JCAP **0310**, 009 (2003ah) [arXiv:hep-ph/0307244].

[48] I. Gil-Botella and A. Rubbia, "Decoupling supernova and neutrino oscillation physics with LAr TPC detectors," arXiv:hep-ph/0404151.

[49] D.B. Cline, K. Lee, Y.H. Seo and P.F. Smith, "Study of the Backgrounds for the Search for Proton Decay at 10^{35} Y at the WIPP Site with the LANNDD Detector", axXiv:astro-ph/0208381

[50] D.B. Cline, Y.H. Seo and F. Sergiampietri, "Mini-LANNDD T40: A detector to measure the neutrino argon cross section and the nu/e containation in the off-axis NuMI beam", arXiv:astro-ph/0301545

[51] F. Sergiampietri, "Near Liquid Argon TPC Detectors for Near Future", Proceedings of NuFact03, in print

[52] F. Sergiampetri, presentation at the Fermilab Liquid Argon Workshop, April 10, 2003

[53] R. Schmitt, "Cryogenic System Estimate for T40 Mini-LANNDD"

[54] A Precise Determination of Electroweak Parameters in Neutrino-Nucleon Scattering, NuTeV Collaboration, Phys.Rev.Lett. 88 091802, 2002

[55] G. Carugno, B. Dainese, F. Pietropaolo and F. Ptohos, "Electron Lifetime Detector for Liquid Argon", Nucl. Instrum. Meth. A **292** (1990) 580

[56] H. Ejiri, et al., http://www.rcnp.osaka-u.ac.jp∼ejiri/DBD-Lett

[57] H. Ejiri, Phys. Rep. **C 338** (2000) 265.

[58] H. Ejiri, J. Engel, R. Hazama, P. Krastev, N. Kudomi, and R.G.H. Robertson, Phys. Rev. Lett. **85** (2000) 2917.

[59] R.G.H. Robertson, *Prog. Part. Nucl. Phys.* 40 (1998) 113.

[60] M.D. Edmiston and C.R. Gruhn, "Energy resolution considerations in Liquid Ionization Chambers", IEEE Trans. Nucl. Sci. **NS-25** (1978) 352

[61] V. D. Ashitkov *et al.*, "A liquid-argon ionization detector for the study of double beta decay," Instrum. Exp. Tech. **46**, 153 (2003) [Prib. Tekh. Eksp. **46N2**, 16 (2003)].